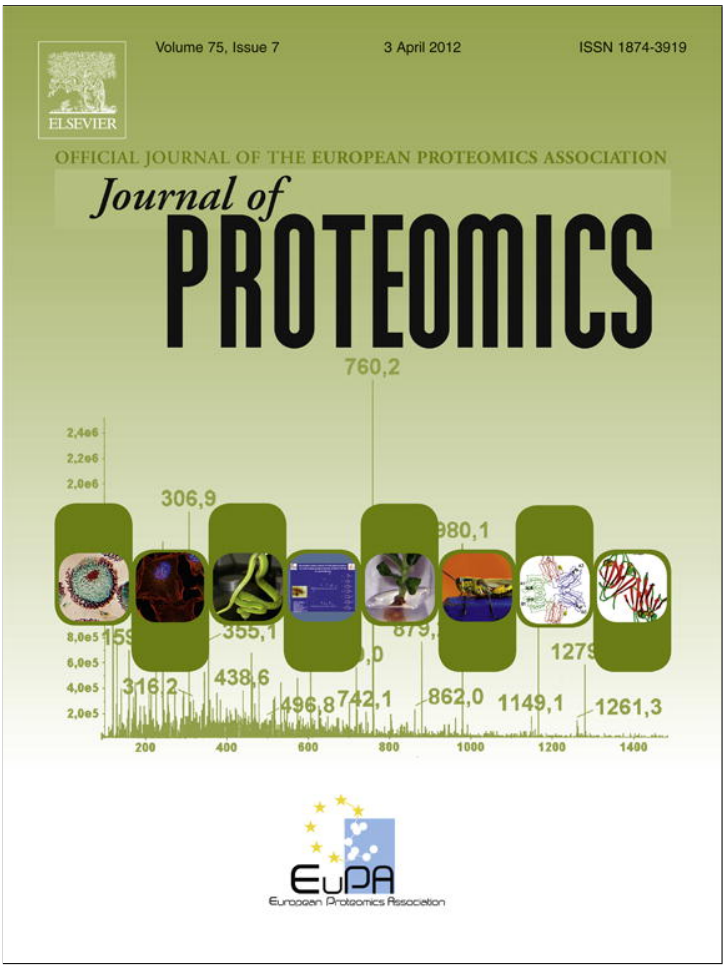

JOURNAL OF PROTEOMICS 75 (2012) 1991–2014

Available online at www.sciencedirect.com

SciVerse ScienceDirect

www.elsevier.com/locate/jprot

Proteomic analysis of UVB-induced protein expression- and redox-dependent changes in skin fibroblasts using lysine- and cysteine-labeling two-dimensional difference gel electrophoresis

Chieh-Lin Wu[a,1], Hsiu-Chuan Chou[b,1], Chao-Sheng Cheng[a], Ji-Min Li[a], Szu-Ting Lin[a], Yi-Wen Chen[a], Hong-Lin Chan[a,*]

[a]Institute of Bioinformatics and Structural Biology & Department of Medical Sciences, National Tsing Hua University, Hsinchu, Taiwan
[b]Department of Applied Science, National Hsinchu University of Education, Hsinchu, Taiwan

ARTICLE INFO

Article history:
Received 2 November 2011
Accepted 27 December 2011
Available online 6 January 2012

Keywords:
Skin fibroblasts
UVB
Redox
Proteomics
DIGE
MALDI-TOF

ABSTRACT

UVB is the most energetic and DNA-damaging to humans in ultraviolet radiation. Previous research has suggested that exposure to UVB causes skin pathologies because of direct DNA damage and the generation of reactive oxygen species (ROS). However, the detailed molecular mechanisms by which UVB leads to skin cancer have yet to be clarified. In the current study, normal skin fibroblast cells (CCD-966SK) were exposed to various doses of UVB, and the changes in protein expression and thiol reactivity were monitored with lysine- and cysteine-labeling 2D-DIGE and MALDI-TOF mass spectrometry. Our proteomic analysis revealed that 89 identified proteins showed significant changes in protein expression, and 37 in thiol reactivity. Many proteins that are known to be involved in protein folding, redox regulation and nucleotide biosynthesis were up-regulated under UVB irradiation. In contrast, proteins responsible for biosynthesis and protein degradation were down-regulated. In addition, the thiol-reactivity of proteins involving cytoskeleton, metabolism, and signal transduction were altered by UVB. In summary, these UVB-modulated cellular proteins and redox-regulated proteins might play important roles in the early stages of skin cancer formation and photoaging induced by UVB-irradiation. Such proteins might provide a potential target for the rational design of drugs to prevent UVB-induced diseases.

1. Introduction

One of the most important functions of the human skin is protection against solar ultraviolet (UV) irradiation which causes pathological changes in the skin such as sunburn, photoaging and even skin cancer. The previous studies indicated that UVC and part of UVB are absorbed by ozone layer, whereas most UVB and UVA are able to reach earth surface, in which,

Abbreviations: 1-DE, one-dimensional gel electrophoresis; 2-DE, two-dimensional gel electrophoresis; Ab, antibody; CCB, colloidal coomassie blue; CHAPS, 3-[(3-cholamidopropyl)-dimethylammonio]-1-propanesulfonate); ddH_2O, double deionized water; DIGE, differential gel electrophoresis; DTT, dithiothreitol; FCS, fetal calf serum; IP-WB, immunoprecipitation–immunoblotting; MALDI-TOF MS, matrix assisted laser desorption ionization-time of flight mass spectrometry; NP-40, Nonidet P-40; TFA, trifluoroacetic acid; UVB, Ultraviolet B.

* *Corresponding author at:* Institute of Bioinformatics and Structural Biology & Department of Medical Sciences, National Tsing Hua University, No.101, Kuang-Fu Rd. Sec.2, Hsin-chu, 30013, Taiwan. Tel.: +886 3 5742476; fax: +886 3 5715934.
E-mail address: hlchan@life.nthu.edu.tw (H.-L. Chan).
[1] These authors contributed equally to this work.

1874-3919/$ – see front matter © 2011 Elsevier B.V. All rights reserved.
doi:10.1016/j.jprot.2011.12.038

UVB is mainly considered to be involve in skin cancer [1–3]. However, the molecular and biochemical mechanisms that lead to skin cancer by UV are yet to be clarified. Recent reports showed that UV-induced reactive oxidant species (ROS) which can activate growth factor receptors, cytokine receptors as well as intracellular signaling molecules [4–6]. The high concentrations of ROS are mediators of damage to cell structures such as plasma membranes, lipid and nucleic acids and play a powerful role to promote tumorigenesis [7,8]. Although the ROS can be balanced by cellular antioxidant reactions such as glutathione detoxification [9], oxidative damage accumulates during the ROS attack and ROS-mediated modifications on biomolecules such as DNA, lipids and proteins have been proposed to contribute in the development of many degenerative diseases and cancers [10].

Several chemical moieties have been found to be potential targets ROS in cells. One of these, the free thiol group (RSH) of cysteine residues is a potent nucleophilic agent and can undergo a number of redox-induced modifications under physiological conditions. Oxidative modifications of RSH groups other than disulphide formation include the formation of the sulfenic acid, sulfinic acid and sulfonic acid depending upon the oxidative capacity of the oxidant [11]. Oxidation of RSH groups to sulfinic and sulfonic acids is irreversible under physiologic conditions and induces loss of biological functions of proteins [12,13].

Two-dimensional gel electrophoresis (2-DE) is one of the most widely used proteomic separation methods which has often been employed for the analysis of differential protein expression in biological samples [14,15]. However, as most users realize, 2-DE and the methods commonly used for in-gel protein visualization are inherently variable and many replicate gels must be run before significant differences in protein expression can be ascribed with accuracy. Moreover, these protein visualization methods often have narrow linear dynamic ranges of detection, making them unsuitable for the analysis of biological samples where protein copy numbers vary enormously. A significant improvement in the ability to use gel-based methods for protein quantitation and detection was achieved with the introduction of 2D-difference gel electrophoresis (2D-DIGE), which enables co-detection of several samples on the same 2-DE gel, so avoiding gel-to-gel variation [16–20].

In the present study, the cellular targets of UVB-irradiation of skin fibroblasts were monitored by lysine- and cysteine-labeling 2D-DIGE [21,22]. These strategies combined with MALDI-TOF MS were used to determine whether cellular protein abundance and thiol reactivity were altered. The results demonstrated a number of differentially labeled proteins that were identified from 2-DE by MS. Using lysine and cysteine 2D-DIGE, this study revealed some of the players involved in the cellular response to UV-B irradiation.

2. Materials and methods

2.1. Chemicals and reagents

Generic chemicals were purchased from Sigma-Aldrich (St. Louis, USA), while reagents for lysine-2D-DIGE were purchased from GE Healthcare (Uppsala, Sweden). The synthesis of the ICy3 and ICy5 dyes has been previously reported [23,24]. All primary antibodies were purchased from Abcam (Cambridge, UK) and anti-mouse, and anti-rabbit secondary antibodies were purchased from GE Healthcare (Uppsala, Sweden). All the chemicals and biochemicals used in this study were of analytical grade.

2.2. Cell lines and cell cultures

The human skin fibroblast line CCD-966SK was purchased from American Type Culture Collection (ATCC), Manassas, VA. CCD-966SK was maintained in Dulbecco's Modified Eagle's medium (DMEM) supplemented with 10% (v/v) fetal calf serum (FCS), L-glutamine (2 mM), streptomycin (100 μg/mL), and penicillin (100 IU/mL) (all from Gibco-Invitrogen Corp., UK). All cells were incubated at 37 °C and 5% CO_2.

2.3. UV-B treatment of skin fibroblast

Before UV-B irradiation, CCD-966SK cells were trypsinized, counted using a hemocytometer and 10^6 cells were seeded into 10 cm-cell culture dishes; after overnight incubation medium was removed and the monolayers were irradiated with indicative UV-B doses in a CL-1000 UV cross-linker (Ultra-Violet Products) fitted with 5×8 W 302 nm dual bipin discharge type tubes. Control cultures were decanted and sham irradiated. After UV-B irradiation, the cultures were filled with fresh medium and continued culture for indicated times.

2.4. MTT cell viability assay

CCD-966SK cells growing exponentially were trypsinized, counted using a hemocytometer and 5000 cells/well were seeded into 96-well plates. The culture was then incubated for 24 h before treatment with indicative doses of UVB or left untreated. After removal of the medium, 50 μL of MTT working solution (1 mg/mL) (Sigma) was added to the cells in each well, followed by a further incubation at 37 °C for 4 h. The supernatant was carefully removed; 100 μL of DMSO was added to each well and the plates shaken for 20 min. The absorbance of samples was then measured at a wavelength of 540 nm in a multi-well plate reader. Values were normalized against the untreated samples and were averaged from 8 independent measurements.

2.5. Assay for endogenous reactive oxygen species using DCFH-DA

CCD-966SK cells growing exponentially were trypsinized, counted using a hemocytometer and 10,000 cells/well were seeded into multiple 24-well plates. The culture was then incubated for 24 h before treatment with indicative doses of UV-B or left untreated. After two washes with PBS, cells were treated with 10 μM of 2,7-dichlorofluorescin diacetate (DCFH-DA; Molecular Probes) at 37 °C for 20 min, and subsequently washed with PBS. Fluorescence was recorded at an excitation wavelength 485 nm and emission wavelength at 530 nm.

2.6. Sample preparation for total cellular protein and thiol reactivity analysis

For total cellular protein analysis, cells were washed in chilled 0.5× PBS and scraped in 2-DE lysis buffer containing 4% w/v CHAPS, 7 M urea, 2 M thiourea, 10 mM Tris–HCl, pH8.3, 1 mM EDTA. Lysates were homogenized by passage through a 25-gauge needle 10 times, insoluble material was removed by centrifugation at 13,000 rpm for 30 min at 4 °C, and protein concentrations were determined using Coomassie Protein Assay Reagent (BioRad). Protein samples were labeled with N-hydroxy succinimidyl ester-derivatives of the cyanine dyes Cy2, Cy3 and Cy5. Briefly, 150 μg of protein sample was minimally labeled with 375 pmol of either Cy3 or Cy5 for comparison on the same 2-DE. To facilitate image matching and cross-gel statistical comparison, a pool of all samples was also prepared and labeled with Cy2 at a molar ratio of 2.5 pmol Cy2/μg of protein as an internal standard for all gels. Thus, the triplicate samples and the internal standard could be run and quantify on multiple 2-DE. The labeling reactions were performed in the dark on ice for 30 min and then quenched with a 20-fold molar ratio excess of free L-lysine to dye for 10 min. The differentially Cy3- and Cy5-labeled samples were then mixed with the Cy2-labeled internal standard and reduced with dithiothreitol for 10 min. IPG buffer, pH3–10 nonlinear (2% (v/v), GE Healthcare) was added and the final volume was adjusted to 450 μL with 2D-lysis buffer for rehydration. All samples were run in triplicate against the standard pool.

For redox DIGE analysis, cells were lysed in 2-DE buffer (4% w/v CHAPS, 8 M urea, 10 mM Tris–HCl pH 8.3 and 1 mM EDTA) in the presence of ICy3 or ICy5 (80 pmol/mg protein) on ice to limit post-lysis thiol modification. Test samples were labeled with the ICy5 dye and mixed with an equal amount of a standard pool of both samples labeled with ICy3. Since ICy dyes interfered with the protein assay, protein concentrations were determined on replica lysates not containing dye. Lysates were left in the dark for 1 h followed by labeling with Cy2 to monitor protein level. The reactions were quenched with DTT (65 mM final concentration) for 10 min followed by L-lysine (20-fold molar ratio excess of free L-lysine to Cy2 dye) for a further 10 min. Volumes were adjusted to 450 μL with buffer plus DTT and IPG buffer for rehydration. All samples were run in triplicate against the standard pool.

The rehydration process was performed with immobilized non-linear pH gradient (IPG) strips (pH3–10, 24 cm) which were later rehydrated by CyDye-labeled samples in the dark at room temperature overnight (at least 12 h). Isoelectric focusing was then performed using a Multiphor II apparatus (GE Healthcare) for a total of 62.5 kV-h at 20 °C. Strips were equilibrated in 6 M urea, 30% (v/v) glycerol, 1% SDS (w/v), 100 mM Tris–HCl (pH8.8), 65 mM dithiothreitol for 15 min and then in the same buffer containing 240 mM iodoacetamide for another 15 min. The equilibrated IPG strips were transferred onto 26×20 cm 12.5% polyacrylamide gels casted between low fluorescent glass plates. The strips were overlaid with 0.5% (w/v) low melting point agarose in a running buffer containing bromophenol blue. The gels were run in an Ettan Twelve gel tank (GE Healthcare) at 4 W/gel at 10 °C until the dye front had completely run off the bottom of the gels. Afterward, the fluorescence 2-DE was scanned directly between the low fluorescent glass plates using an Ettan DIGE Imager (GE Healthcare). This imager is a charge-coupled device-based instrument that enables scanning at different wavelengths for Cy2-, Cy3-, and Cy5-labeled samples. Gel analysis was performed using DeCyder 2-D Differential Analysis Software v7.0 (GE Healthcare) to co-detect, normalize and quantify the protein features in the images. Features detected from non-protein sources (e.g. dust particles and dirty backgrounds) were filtered out. Spots displaying a ≧1.5 average-fold increase or decrease in abundance with a p-value <0.05 were selected for protein identification.

2.7. Protein staining

Colloidal coomassie blue G-250 staining was used to visualize CyDye-labeled protein features in 2-DE. Bonded gels were fixed in 30% v/v ethanol, 2% v/v phosphoric acid overnight, washed three times (30 min each) with ddH_2O and then incubated in 34% v/v methanol, 17% w/v ammonium sulfate, 3% v/v phosphoric acid for 1 h, prior to adding 0.5 g/L coomassie blue G-250. The gels were then left to stain for 5–7 days. No destaining step was required. The stained gels were then imaged on an ImageScanner III densitometer (GE Healthcare), which processed the gel images as .tif files.

2.8. In-gel digestion

Excised post-stained gel pieces were washed three times in 50% acetonitrile, dried in a SpeedVac for 20 min, reduced with 10 mM dithiothreitol in 5 mM ammonium bicarbonate pH 8. 0 (ammonium bicarbonate) for 45 min at 50 °C and then alkylated with 50 mM iodoacetamide in 5 mM ammonium bicarbonate for 1 h at room temperature in the dark. The gel pieces were then washed three times in 50% acetonitrile and vacuum-dried before reswelling with 50 ng of modified trypsin (Promega) in 5 mM ammonium bicarbonate. The pieces were then overlaid with 10 μl of 5 mM ammonium bicarbonate and trypsinized for 16 h at 37 °C. Supernatants were collected, peptides were further extracted twice with 5% trifluoroacetic acid in 50% acetonitrile and the supernatants were pooled. Peptide extracts were vacuum-dried, resuspended in 5 μL ddH_2O, and stored at −20 °C prior to MS analysis.

2.9. Protein identification by MALDI-TOF MS and MS/MS

For protein identification, extracted peptides were subjected to peptide mass fingerprinting (PMF) using MALDI-TOF MS. Briefly, 0.5 μL of trypsin digested protein sample was mixed with 0.5 μL of a matrix solution containing α-cyano-4-hydroxycinammic acid at a concentration of 1 mg/mL of 50% ACN/0.1% TFA (v/v), spotted onto an anchorchip target plate (Bruker Daltonics) and dried. The peptide mass fingerprints were acquired using an Autoflex III mass spectrometer (Bruker Daltonics) in reflector mode and the raw data was analyzed with FlexAnalysis acquisition software (version 3.0, Bruker Daltonics). The algorithm used for spectral annotation was SNAP (Sophisticated Numerical Annotation Procedure). The following metrics were used: peak detection algorithm: SNAP; signal to noise threshold: 25; relative intensity threshold: 0%; minimum intensity threshold:

0; maximal number of peaks: 50; quality factor threshold: 1000; SNAP average composition: averaging; baseline subtraction: median; flatness: 0.8; median level: 0.5. The spectrometer was also calibrated with a peptide calibration standard (Bruker Daltonics) and internal calibration was performed using trypsin autolysis peaks at *m/z* 842.51 and *m/z* 2211.10 (MS BioTools version 3.0, Bruker Daltonics). Peaks in the mass range of *m/z* 800–3000 were used to generate a peptide mass fingerprint that was searched against the Swiss-Prot/TrEMBL database (2010_04 of 23-Mar-10, 515,203 sequence entries) using Mascot software v2.3.00 (Matrix Science, London, UK). The following parameters were used: *Homo sapiens*; tryptic digest with a maximum of 1 missed cleavage; carbamidomethylation of cysteine, partial protein N-terminal acetylation, partial methionine oxidation, partial modification of glutamine to pyroglutamate, ICy3 (C34 H44 N3 O) and ICy5 (C34 H42 N3 O) and a mass tolerance of 50 ppm. Identifications were accepted based on significant MASCOT scores ($P<0.05$), at least 4 peptides per protein, spectral annotation and observed versus expected molecular weight and p*I* on 2-DE. MALDI-TOF/TOF analysis was performed on the same instrument using the LIFT mode. MS/MS ion searches were performed using Mascot with the same search parameters as above and using an MS/MS tolerance of ±0.2 Da.

2.10. *Immunoblotting*

Immunoblotting was used to validate the differential expression of mass spectrometry identified proteins. Cells were lysed with a lysis buffer containing 50 mM HEPES pH 7.4, 150 mM NaCl, 1% NP40, 1 mM EDTA, 2 mM sodium orthovanadate, 100 μg/mL AEBSF, 17 μg/mL aprotinin, 1 μg/mL leupeptin, 1 μg/mL pepstatin, 5 μM fenvalerate, 5 μM BpVphen and 1 μM okadaic acid prior to protein quantification with Coomassie Protein Assay Reagent (BioRad). 30 μg of protein samples were diluted in Laemmli sample buffer (final concentrations: 50 mM Tris pH 6.8, 10% (v/v) glycerol, 2% SDS (w/v), 0.01% (w/v) bromophenol blue) and separated by 1D-SDS-PAGE following standard procedures. After electroblotting separated proteins onto 0.45 μm Immobilon P membranes (Millipore), the membranes were blocked with 5% w/v skim milk in TBST (50 mM Tris pH 8.0, 150 mM NaCl and 0.1% Tween-20 (v/v)) for 1 h. Membranes were then incubated in primary antibody solution in TBS-T containing 0.02% (w/v) sodium azide for 2 h. Membranes were washed in TBS-T (3×10 min) and then probed with the appropriate horseradish peroxidase-coupled secondary antibody (GE Healthcare). After further washing in TBS-T, immunoprobed proteins were visualized using an enhanced chemiluminescence method (Visual Protein Co.).

2.11. *Validation of thiol reactivity changes by immunoprecipitation coupled immunoblotting*

UV-B irradiated CCD-966SK cells were lysed in the presence of ICy3 or ICy5 dyes to limit postlysis-induced thiol modification. The labeling reactions were performed in the dark in 37 °C for 1 h and then quenched with a 2-fold molar ratios of DTT for 10 min. 500 μg of ICy dye-labeled cell lysates were 20 folds-diluted with NP40 buffer containing protease inhibitors and then incubated with 5 μg primary antibody and 40 μL of a 50% slurry of protein A-Sepharose for 16 h at 4 °C. Immune complexes were then washed three times in lysis buffer and boiled in Laemmli sample buffer prior to resolve with SDS-PAGE. Afterward, the ICy3 or ICy5 images were scanned directly between the low fluorescent glass plates using an Ettan DIGE Imager (GE Healthcare) followed by immunoblotting analysis with the same primary antibody to detect the specific protein. The immunoblotting procedures were described above.

3. Result

3.1. *UVB-induced shifts in protein expression profiles in human skin fibroblast CCD-966SK cells*

To study the effect of UVB irradiation on the expression of skin fibroblast proteins, CCD-966SK cells were exposed to

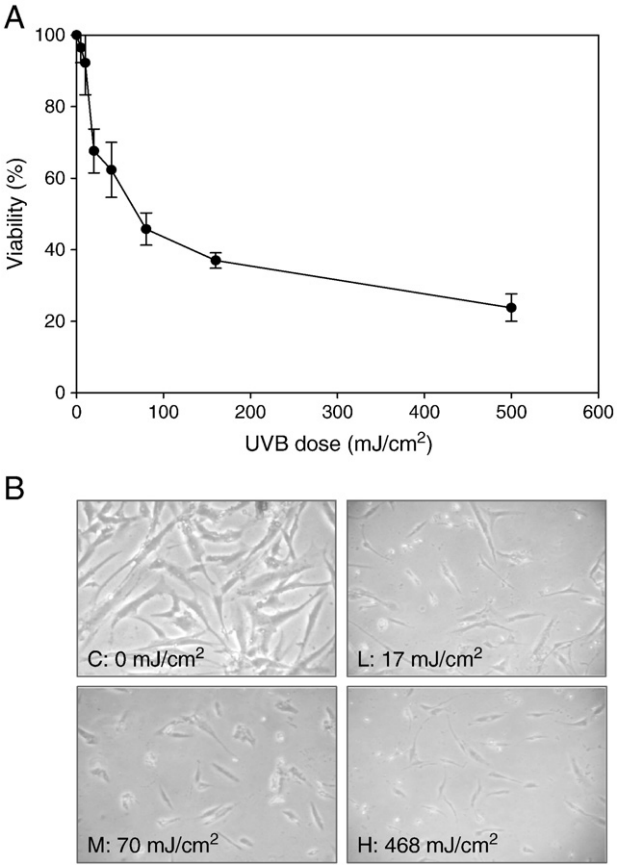

Fig. 1 – UVB-induced loss of cell viability and cell morphologic changes. (A) MTT-based viability assays were performed where 10,000 CCD-966SK cells were plated into 96-well plates in medium containing 10% FBS. After 24 h, the cells were irradiated with the indicated doses of UVB for indicated doses. Cells were incubated with MTT and then DMSO added and the plates shaken for 20 min followed by measurement of the absorbance at 540 nm. Values were normalized against untreated samples and are the average of 4 independent measurements ± the standard deviation. (B) The morphological changes of CCD-966SK cells were photographed at the UVB doses indicated. Each treatment condition has been performed at least 3 times.

302 nm dual bipin discharge type UVB tubes for indicated UVB doses. As expected from the dosage used, irradiation of CCD-966SK cells to UVB was shown to result in a dose-dependent loss of cell viability (Fig. 1A). At UVB doses of 17 mJ/cm^2, 70 mJ/cm^2 and 468 mJ/cm^2, a significant loss of cell viability (25%, 50%, 75%) and change in cell morphology was detectable after 24 h incubation, respectively (Fig. 1B).

CCD-966SK cells obtained at 24 h after low dose (17 mJ/cm^2), middle dose (70 mJ/cm^2) and high dose (468 mJ/cm^2) UVB irradiation or unirradiated. A total of four cell lysate samples were analyzed by 2D-DIGE to examine the protein expression changes in various doses of UVB irradiation and unirradiated CCD-966SK cells. The analysis revealed 1911 protein spots were detected and 200 protein features that displayed differential expression ($\geqq$1.5-fold; $P<0.05$) across the 4 different conditions (Fig. 2). Proteins in 89 of these features were subsequently identified by MALDI-TOF MS (Table 1). These differentially expressed proteins are mostly located in cytoplasm, nucleus and endoplasmic reticulum and have functions in protein folding, signaling, cytoskeleton regulation and protein biosynthesis (Fig. 3 and Table 2).

To further verify the up- or down-regulation of the identified proteins, we performed immunoblotting and ELISA analysis of some of the proteins we found modulated by UVB irradiation in CCD-966SK cells compared with control cells without UVB-irradiation (Fig. 4). Among these, we used specific antibodies against HSP-27, cyclophilin A, peroxiredoxin 4, cofilin-1, prohibitin and annexin A2. Fig. 4 reveals that most of the above verified proteins showed the same pattern of expression with the 2D-DIGE analysis (Table 1). These results also strengthen the validation of 2D-DIGE analysis in this study.

3.2. *Redox proteomic analysis of UVB-induced cysteine modifications of CCD-966SK proteins*

UVB has been reported to induce ROS mediating cell damages and promoting tumorigenesis. Although the low concentration of ROS can be balanced by cellular antioxidant reactions, accumulation of ROS mediates modifications on biomolecules such as DNA, lipids and proteins in cells. The free thiol group of cysteine residues is a potent nucleophilic agent to undergo a number of oxidative modifications leading to loss of biological functions of proteins (see Introduction). In order to optimize the condition to monitor oxidative modifications, DCF fluorescence was used to detect ROS production induced by UVB-irradiation. The result revealed that irradiation of CCD-966SK cells with UVB for 20 min resulted in a dose-dependent increase in ROS generation compared with

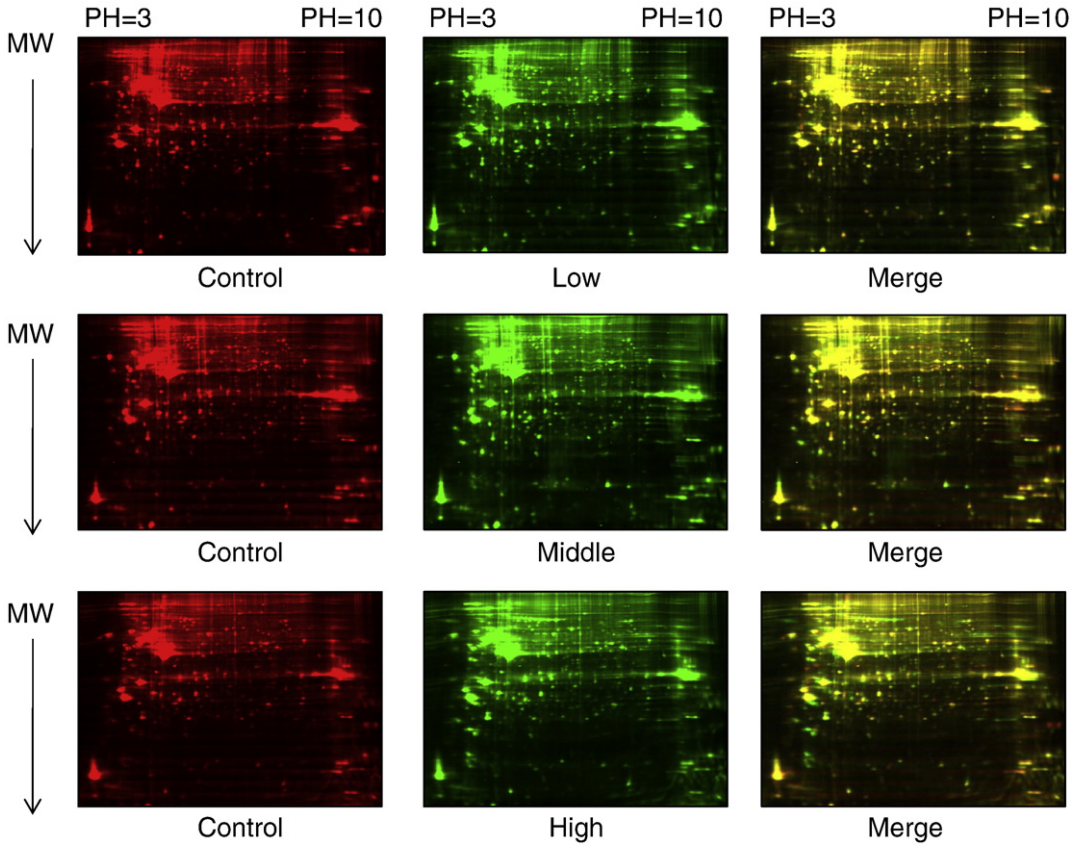

Fig. 2 – 2D-DIGE analysis of UVB-dependent differentially expressed proteins in CCD-966SK cells. UVB-irradiated CCD-966SK cells were lysed and arranged for a triplicate 2D-DIGE experiment. Protein samples (50 μg each) were labeled with Cy-dyes and separated using 24 cm, pH 3–10 non-linear IPG strips. 2D-DIGE images of the protein samples from untreated and UVB-irradiated CCD-966SK cells at low dose (17 mJ/cm^2), middle dose (70 mJ/cm^2) and high dose (468 mJ/cm^2) were shown as well as overlaid pseudo-colored image processed with ImageQuant Tool (GE Healthcare).

Table 1 – Alphabetic list of identified differentially expressed proteins after 2D-DIGE coupled with MALDI-TOF mass spectrometry analysis in CCD-966SK cells in response to UVB irradiation.

Spot no.	Swiss-prot no.	Protein name	MW	pI	No. matched peptides	Score	Cov. (%)	Low / control[a]	Middle / control[a]	High / control[a]	Matched peptides	Subcellular location	Functional class
1362	P62258	14-3-3 protein epsilon	29,326	4.63	8/14	74/56	22%	-1.02	-1.63	-1.16	MDDREDLVYQAK, LAEQAER	Cytoplasm	Signal transduction
975	Q9UNM6	26S proteasome non-ATPase regulatory subunit 13	43,176	5.53	7/17	70/56	16%	-1.04	-1.69	-1.18	LYENFISEFEHR, YYQTIGNHASYYK	Cytoplasm	Protein degradation
1054	P08865	40S ribosomal protein SA	32,947	4.79	8/20	81/56	41%	-1.2	-1.68	-1.51	AIVAIENPADVSVISSR, FAAATGATPIAGR	Cytoplasm	Protein biosynthesis
1158	P05388	60S acidic ribosomal protein P0	34,423	5.71	4/11	64/56	18%	-1.08	-1.54	-1.09	QMQQIR, GHLENNPALEK	Cytoplasm	Protein biosynthesis
1427	O95336	6-phosphogluconolactonase	27,815	5.7	4/9	70/56	18%	-1.08	1.78	1.06	WTLGFCDER, LVPFDHAESTYGLYR	Cytoplasm	Metabolism
333	P11021	78 kDa glucose-regulated protein	72,402	5.07	7/17	71/56	12%	-1.21	1.34	-1.56	ITPSYVAFTPEGER, KVTHAVVTVPAYFNDAQR	ER	Protein folding
1900	P11021	78 kDa glucose-regulated protein	72,402	5.07	6/15	60/56	11%	-1.28	1.56	-1.35	ITPSYVAFTPEGER, KVTHAVVTVPAYFNDAQR	ER	Protein folding
797	P61158	Actin-related protein 3	47,797	5.61	8/21	86/56	26%	1.09	-1.06	1.53	HGIVEDWDLMER, AEPEDHYFLLTEPPLNTPENR	Cytoplasm	Cytoskeleton
1028	O95433	Activator of 90 kDa heat shock protein ATPase homolog 1	38,421	5.41	6/13	58/56	14%	1.27	-1.41	-1.59	WIVEER, ADATNVNNWHWTER	Cytoplasm	Protein folding
1081	P14550	Alcohol dehydrogenase [NADP+]	36,892	6.32	5/12	68/56	17%	1.64	2.17	1.11	YALSVGYR, GLVQALGLSNFNSR	Cytoplasm	Metabolism
1198	P07355	Annexin A2	38,808	7.57	13/32	119/56	37%	-1.14	-1.16	-1.56	MSTVHEILCK, LSLEGDHSTPPSAYGSVK	Plasma membrane	Signal transduction/Ca regulation
1201	P07355	Annexin A2	38,808	7.57	14/31	126/56	35%	-1.02	-1.29	-1.91	LSLEGDHSTPPSAYGSVK, AYTNFDAER	Plasma membrane	Signal transduction/Ca regulation
1285	P08758	Annexin A5	35,971	4.94	6/19	64/56	21%	1.11	-1.18	1.9	GTVTDFPGFDER, GLGTDEESILTLLTSR	Plasma membrane	Signal transduction/Ca regulation
460	P31939	Bifunctional purine biosynthesis protein PURH	65,089	6.27	7/15	73/56	13%	-1.01	1.14	1.7	TGLVEFAR, TLHPAVHAGILAR	Cytoplasm	Nucleotide biosynthesis
1452	P04632	Calpain small subunit 1	28,469	5.05	5/13	67/56	24%	-1.09	1.75	-1.44	R.ILGGVISAISEAAAQYNPEPPPPR. T, R.THYSNIEANESEEVR.Q	Cytoplasm	Cell migration
735	P27797	Calreticulin	48,283	4.29	6/21	63/56	16%	-1.33	1.64	-1.2	EQFLDGDGWTSR, FYALSASFEPFSNK	ER	Protein folding
686	P27797	Calreticulin	48,283	4.29	7/23	70/56	18%	-1.37	1.6	-1.11	EQFLDGDGWTSR, FYALSASFEPFSNK	ER	Protein folding
1811	P29373	Cellular retinoic acid-binding protein 2	15,854	5.42	4/14	58/56	39%	1.7	1.77	-1.61	MPNFSGNWK, VLGVNVMLR	Cytoplasm	Transport
1334	O14579	Coatomer subunit epsilon	34,688	4.97	5/12	70/56	17%	-1.01	-1.53	-1.22	NAFYIGSYQQCINEAQR, DVFLYR	Golgi	Vascular transport
1730	P23528	Cofilin-1	18,719	8.22	5/16	60/56	36%	-1.19	3.57	-1.51	VFNDMKVR, .EILVGDVGQTVDDPYATFVK	Cytoplasm	Cell migration
1852	Q14993	Collagen alpha-1(XIX) chain	115,947	8.57	6/13	58/56	8%	1.07	-1.93	1.33	LGSALLIR, VVEFMFQATEGDVLNYIFRNR	Secreted	Cell-cell interaction

1348	Q9Y6G9	Cytoplasmic dynein 1 light intermediate chain 1	56829	6.01	5/9	63/56	11%	1.44	1.22	1.67	QMEQKLIR, NIDLVYK	Cytoplasm	Cell migration
15	O75925	E3 SUMO-protein ligase PIAS1	72760	6.9	6/14	63/56	9%	-1.89	-1.81	-2.12	MADSAELKQMVMSLR, ADSAELKQMVMSLR	Nucleus	Protein degradation
822	P26641	Elongation factor 1-gamma	50429	6.25	12/31	96/56	25%	1.12	1.59	-1.43	K.ALIAAQYSGAQVR.V, R.VLSAPPHFHFGQTNR.T	Cytoplasm	Protein biosynthesis
1424	P30040	Endoplasmic reticulum protein ERp29	29032	6.77	7/14	93/56	26%	-1.18	1.32	-2	FDTQYPYGEK, ESYPVFYLFR	ER	Protein folding
1890	Q7L2H7	Eukaryotic translation initiation factor 3 subunit M	42932	5.41	5/9	68/56	14%	-1.08	-1.86	1.56	LQLLSNLFHGMDK, YTVYCSLIK	Cytoplasm	Protein biosynthesis
656	Q16658	Fascin	55123	6.84	6/15	63/56	14%	1.15	1.44	3.4	FLIVAHDDGR, WSLQSEAHRR	Cytoplasm	Cell migration
342	Q96AY3	FK506-binding protein 10	64717	5.36	8/22	70/56	18%	-1.83	1.05	-1.27	ASPAGGPLEDVVIER, NTLVAIVVGVGR	ER	Protein folding
456	O95302	FK506-binding protein 9	63500	4.91	5/11	68/56	9%	-1.45	1.6	1.32	YHYVGTFPDGQK, TIQVSDFVR	ER	Protein folding
1887	P04075	Fructose-bisphosphate aldolase A	39851	8.3	9/23	102/56	33%	-1.03	1.02	-1.54	PYQYPALTPEQK, QLLLTADDR	Cytoplasm	Metabolism
552	P14136	Glial fibrillary acidic protein	49907	5.42	5/10	62/56	19%	-1.14	-1.43	2.05	R.MPPPLPTRVDFSLAGALNAGFK. E, K.LQDETNLRLEAENNLAAYR.Q	Cytoplasm	Cell migration
576	P11413	Glucose-6-phosphate 1-dehydrogenase	59675	6.39	6/8	85/56	16%	-1.25	1.05	-1.79	R.DGLLPENTFIVGYAR.S, R.NSYVAGQYDDAASYQR.L	Cytoplasm	Metabolism
1544	P09211	Glutathione S-transferase P	23569	5.43	6/13	94/56	40%	-1.08	1.47	-1.6	MPPYTVVYFPVR, PPYTVVYFPVR	Cytoplasm	Redox regulation
1008	P29992	Guanine nucleotide-binding protein subunit alpha-11	42382	5.51	6/13	59/56	16%	1.63	-1.03	1.44	K.IIYSHFTCATDTENIR.F, R.MEESKALFR.T	Cytoplasm	Signal transduction
385	P11142	Heat shock cognate 71 kDa protein	71082	5.37	6/14	58/56	11%	1.16	1.6	1.16	GPAVGIDLGTTYSCVGVFQHGK, TTPSYVAFTDTER	Cytoplasm	Protein folding
1502	P04792	Heat shock protein beta-1 / HSP-27	22826	5.98	7/29	84/56	28%	-1.45	1.38	-3.18	VPFSLLR, GPSWDPFR	Cytoplasm	Protein folding
1494	P04792	Heat shock protein beta-1 / HSP-27	22826	5.98	6/21	73/56	28%	-1.39	-1.07	-2.83	VPFSLLR, GPSWDPFR	Cytoplasm	Protein folding
1064	P07910	Heterogeneous nuclear ribonucleoproteins C1/C2	33707	4.95	4/5	57/56	13%	-1.11	-1.4	-2.89	SDVEAIFSKYGK, GFAFVQYVNER	Nucleus	Protein biosynthesis
1728	P37235	Hippocalcin-like protein 1	22413	5.21	6/11	92/56	32%	-1.09	1.76	-1.03	LRPEVLQDLR, IYANFFPYGDASK	Cytoplasm	Signal transduction/Ca regulation
911	O75874	Isocitrate dehydrogenase [NADP] cytoplasmic	46915	6.53	6/11	73/56	14%	1.25	1.84	1.89	NILGGTVFR, LVSGWVKPIIIGR	Cytoplasm	Metabolism
554	P08779	Keratin, type I cytoskeletal 16	51578	4.99	16/50	128/56	39%	-1	-6.07	-2.71	VTMQNLNDR, QRPSEIKDYSPYFK	Cytoplasm	Cytoskeleton
	P04264	Keratin, type II cytoskeletal 1	66170	8.15	9/50	61/56	24%	-1	-6.07	-2.71	SGGGFSSGSAGIINYQR, SLNNQFASFIDKVR	Cytoplasm	Cytoskeleton
	P02538	Keratin, type II cytoskeletal 6A	60293	8.09	12/50	73/56	20%	-1	-6.07	-2.71	ASTSTTIR, FASFIDKVR	Cytoplasm	Cytoskeleton
1056	P40121	Macrophage-capping protein	38779	5.88	5/8	60/56	13%	1.54	1.99	1.24	EVQGNESDLFMSYFPR, EVQGNESDLFMSYFPRGLK	Cytoplasm	Cell migration

(*continued on next page*)

Table 1 (*continued*)

Spot no.	Swiss-prot no.	Protein name	MW	pI	No. matched peptides	Score	Cov. (%)	Low / control[a]	Middle / control[a]	High / control[a]	Matched peptides	Subcellular location	Functional class
1732	O14950	Myosin regulatory light chain MRLC2	19824	4.71	5/17	62/56	30%	1.09	1.55	2.3	EAFNMIDQNR, NAFACFDEEATGTIQEDYLR	Cytoplasm	Cell migration
	P19105	Myosin regulatory light chain MRLC3	19839	4.67	5/17	62/56	30%	1.09	1.55	2.3	EAFNMIDQNR, NAFACFDEEATGTIQEDYLR	Cytoplasm	Cell migration
145	Q14697	Neutral alpha-glucosidase AB	107263	5.74	10/30	65/56	11%	-1.12	-1.01	-1.81	SIRPGLSPYR, YRVPDVLVADPPIAR	ER	Protein folding
1857	P06748	Nucleophosmin	32726	4.64	6/14	61/56	22%	-1.13	1.72	-1.73	VDNDENEHQLSLR, MSVQPTVSLGGFEITPPVVLR	Nucleus	Protein folding
371	Q7RTW8	Otoancorin	129534	5.53	7/13	60/56	7%	-1.14	1.29	4.27	ALQSPGVNR, GSSCGSFLQPDITER	Plasma membrane	Adhesion
372	Q7RTW8	Otoancorin	129534	5.53	6/17	56/56	6%	-1.39	1.8	8.09	ALQSPGVNR, GSSCGSFLQPDITER	Plasma membrane	Adhesion
373	Q7RTW8	Otoancorin	129534	5.53	6/21	76/56	6%	1.13	2.33	13.62	ALQSPGVNR, GSSCGSFLQPDITER	Plasma membrane	Adhesion
1899	P62937	Peptidyl-prolyl cis-trans isomerase A	18229	7.68	5/12	61/56	35%	-1.16	1.71	-2.42	VNPTVFFDIAVDGEPLGR, LNCQVIGASVDSHFCHLAWVNTP VSFELFADKVPK	Cytoplasm	Protein folding
1754	P62937	Peptidyl-prolyl cis-trans isomerase A	18229	7.68	5/11	64/56	29%	-1.37	1.64	-2.11	MVNPTVFFDIAVDGEPLGR, VNPTVFFDIAVDGEPLGR	Cytoplasm	Protein folding
1558	Q06830	Peroxiredoxin-1	22324	8.27	5/10	62/56	26%	1.15	1.53	-1.05	K, ADEGISFR TREEECHFYAGGQVYPGEASR,	Cytoplasm	Redox regulation
1471	Q13162	Peroxiredoxin-4	30749	5.86	9/23	105/56	39%	-1.33	1.81	-1.88	EEECHFYAGGQVYPGEASR R.FHDFLGDSWGILFSHPR.D,	Cytoplasm	Redox regulation
1910	P30041	Peroxiredoxin-6	25133	6	6/20	113/56	34%	-1.2	1.11	-1.67	R.DFTPVCTTELGR.A	Cytoplasm	Redox regulation

427	Q5UE93	Phosphoinositide 3-kinase regulatory subunit 6	85060	7.57	6/13	61/56	9%	1.84	1.3	2.22	R.MVIAEQNLTNELYPYQER.V, R.VSVLSTDSGIER.D	Cytoplasm	Signal transduction
647	Q9UMS4	Pre-mRNA-processing factor 19	55603	6.14	5/12	64/56	17%	1.2	-1.75	-1.17	.MSLICSISNEVPEHPCVSPVSNHV YERR, VAHPIRPKPPSATSIPAILK	Nucleus	Protein biosynthesis
1426	P35232	Prohibitin	29843	5.57	4/9	74/56	21%	-1.1	1.04	1.55	FGLALAVAGGVVNSALYNVDAG HR, ILFRPVASQLPR	Mitochondrion	Growth regulation
1377	Q06323	Proteasome activator complex subunit 1	28876	5.78	5/13	58/56	15%	1.02	1.42	-1.88	K.TENLLGSYFPK.K, K.IVVLLQR.L	Proteasome	Protein degradation
1355	P61289	Proteasome activator complex subunit 3	29602	5.69	4/6	60/56	14%	1.19	-1.48	-1.8	MWVQLLIPR, YPHVEDYR	Proteasome	Protein degradation
1881	P07237	Protein disulfide-isomerase	57480	4.76	10/35	78/56	21%	-1.46	1.53	-1.73	VDATEESDLAQQYGVR, HNQLPLVIEFTEQTAPK	ER	Protein folding
1880	P30101	Protein disulfide-isomerase A3	57146	5.98	8/19	61/56	12%	-1.17	1.76	1.23	QAGPASVPLR, LNFAVASR	ER	Protein folding
1596	Q99497	Protein DJ-1	20050	6.33	4/8	65/56	32%	-1.34	1.35	-1.84	GAEEMETVIPVDVMR, VTVAGLAGKDPVQCSR	Nucleus	Redox regulation
1366	P00491	Purine nucleoside phosphorylase	32325	6.45	5/18	64/56	24%	1.68	-1.41	1.26	HRPQVAIICGSGLGGLTDK, LTQAQIFDYGEIPNFPR	Cytoplasm	Nucleotide biosynthesis
556	P14618	Pyruvate kinase isozymes M1/M2	58470	7.96	5/12	77/56	14%	1.29	1.53	2.09	TATESFASDPILYRPVAVALDTK, FGVEQDVDMVFASFIR	Cytoplasm	Metabolism
988	Q15293	Reticulocalbin-1	38866	4.86	8/22	88/56	31%	1.12	2.27	1.03	TFDQLTPDESKER, IDNDGDGFVTTEELK	ER	Signal transduction/Ca regulation

(*continued on next page*)

Table 1 (*continued*)

Spot no.	Swiss-prot no.	Protein name	MW	pI	No. matched peptides	Score	Cov. (%)	Low / control[a]	Middle / control[a]	High / control[a]	Matched peptides	Subcellular location	Functional class
1038	Q96D15	Reticulocalbin-3	37470	4.74	9/31	81/56	27%	-1.69	1.04	1.61	EFDQLTPEESQAR, AGDGDGWVSLAELR	ER	Signal transduction/Ca regulation
1552	P52565	Rho GDP-dissociation inhibitor 1	23250	5.02	7/20	73/56	20%	-1.01	-1.31	1.6	YKEALLGR, QSFVLKEGVEYR	Cytoplasm	Signal transduction
1017	Q9BZJ4	Solute carrier family 25 member 39	39589	9.68	5/15	60/56	16%	-1.03	-1.42	1.96	R.TAVAQGGWR.S, R.FTGTMDAFVK.I	Mitochondrion	Heme biosynthesis
1139	Q12799	T-complex protein 10A homolog	45668	8.51	8/34	64/56	21%	-2.73	1.54	-3.17	LEGQLEAGEPK, LQSHMDALRK	Cytoplasm	Protein folding
1453	P60174	Triosephosphate isomerase	26938	6.45	7/9	123/56	28%	-1.22	1.37	-2.25	KFFVGGNWK, FFVGGNWK	Cytoplasm	Metabolism
103	Q9NV66	tRNA wybutosine-synthesizing protein 1 homolog	84732	6.42	6/10	54/56	7%	-1.32	-1.01	-1.72	TQGKNLQEK, DIFVSGVK	Nucleus	Protein biosynthesis
1263	Q96IK2	Tropomyosin alpha-1 chain	32746	4.69	9/31	70/56	20%	-2.62	1.02	-3.13	LDKENALDR, ATDAEADVASLNR	Cytoplasm	Cytoskeleton
1362	P67936	Tropomyosin alpha-4 chain	28619	4.67	8/43	57/56	20%	-1.02	-1.63	-1.16	AGLNSLEAVK, EKAEGDVAALNR	Cytoplasm	Cytoskeleton
639	P23381	Tryptophanyl-tRNA synthetase, cytoplasmic	53474	5.83	5/11	76/56	13%	-1.33	-1.63	-1.3	ATGQRPHHFLR, GIFFSHR	Cytoplasm	Protein biosynthesis
1621	P30085	UMP-CMP kinase	22436	5.44	5/14	69/56	35%	1.19	1.73	1.14	K.YGYTHLSAGELLR.D, K.FLIDGFPR.N	Cytoplasm	Nucleotide biosynthesis
1057	Q7L592	UPF0511 protein C2orf56, mitochondrial	49435	8.47	6/12	74/56	18%	1.53	2.08	1.05	STAFQLVELGPGRGTLVGDILR, EKVPLER	Mitochondrion	Unknown
1008	P06132	Uroporphyrinogen decarboxylase	41103	5.77	7/18	64/56	15%	1.63	-1.03	1.44	YLPEFR, AAQDFFSTCR	Cytoplasm	Heme biosynthesis
1051	P08670	Vimentin	53676	5.06	6/18	59/56	15%	-1.34	1.68	3	EKLQEEMLQR, EEAENTLQSFR	Cytoplasm	Cytoskeleton
1685	P08670	Vimentin	53676	5.06	9/24	65/56	15%	1.2	3.46	8.78	VELQELNDR, LGDLYEEEMR	Cytoplasm	Cytoskeleton
1691	P08670	Vimentin	53676	5.06	7/23	56/56	12%	1.09	4.13	10.91	VELQELNDR, DNLAEDIMR	Cytoplasm	Cytoskeleton
1611	P08670	Vimentin	53676	5.06	6/23	71/56	14%	1.02	3.74	15	FADLSEAANR, QESTEYR	Cytoplasm	Cytoskeleton
1492	Q8IYN0	Zinc finger protein 100	64597	9.17	5/10	57/56	11%	-1.01	1.49	1.53	IHTGVKPYK, GFNWSSALTKHK	Nucleus	Gene regulation
1891	O15231	Zinc finger protein 185	49955	5.26	5/12	61/56	12%	-1.05	-1.59	1.54	SEAASGVLRR, TAPREHSYVLSAAK	Nucleus	Gene regulation
1274	O15231	Zinc finger protein 185	49955	5.26	6/13	67/56	14%	1.18	1.11	4.77	SEAASGVLRR, TAPREHSYVLSAAK	Nucleus	Gene regulation
628	Q6ZN57	Zinc finger protein 2 homolog	54360	8.91	6/19	58/56	14%	-1.17	1.76	1.57	TQRMFVGK, HQRIHTGEKPYK	Nucleus	Gene regulation
157	Q9UK13	Zinc finger protein 221	73677	8.87	5/7	67/56	13%	-1.16	1.09	-1.53	LYRDVMLENFR, NLLSVGNQPFHQDTFHFLGK	Nucleus	Gene regulation
245	Q9UK13	Zinc finger protein 221	73677	8.87	5/11	56/56	11%	-1.28	2.34	1.03	NSSQFFKEGDVPCQIEAR, QSISDVSVFDLHQQSHSGEK	Nucleus	Gene regulation

[a]**Average ratio of differential expression ($p < 0.05$) between low dose UVB-irradiation (17 mJ/cm^2)/middle dose UVB-irradiation (70 mJ/cm^2)/high dose UVB-irradiation (468 mJ/cm^2) and untreated cells (Ctrl) calculated from triplicate gels. Gray shaded cells indicate proteins where the changes between UVB irradiation/Ctrl are significantly greater than 1.5-fold differences.**

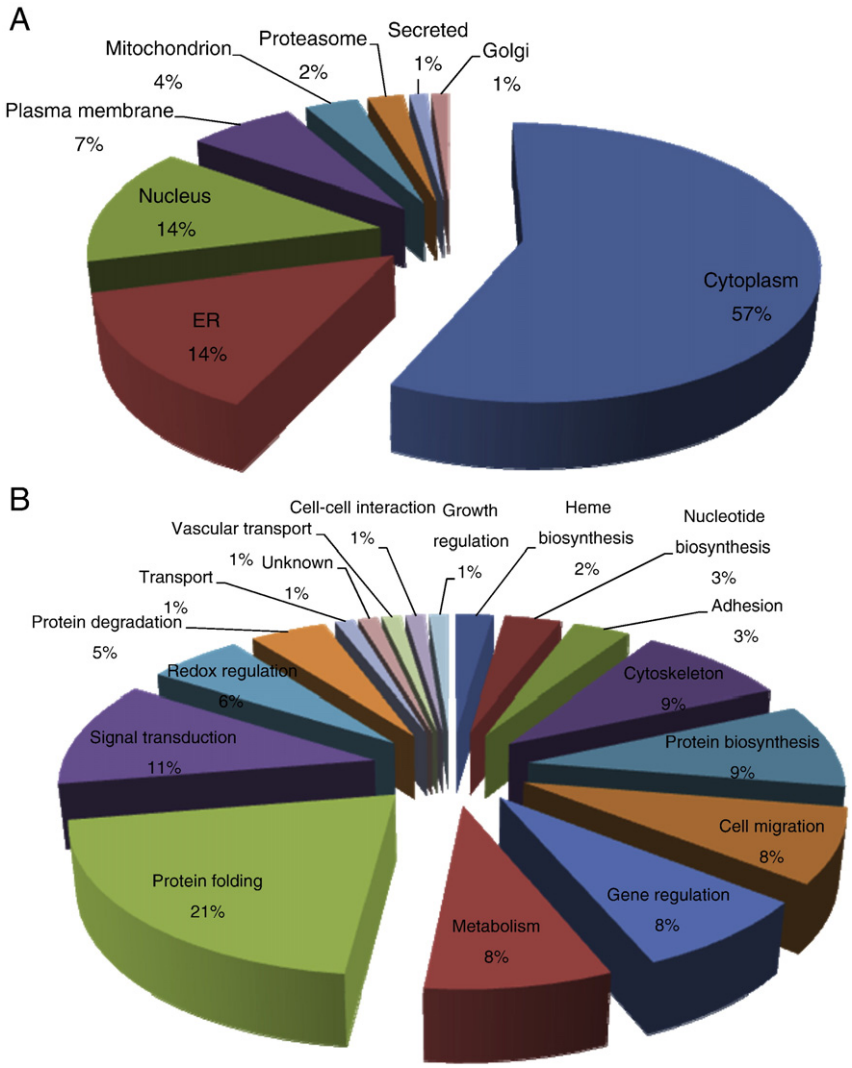

Fig. 3 – Percentage of differentially expressed proteins identified by 2D-DIGE/MALDI-TOF MS for UVB-untreated or -irradiated CCD-966SK cells according to their sub-cellular locations (A) and biological functions (B).

unirradiated CCD-966SK cells (Fig. 5). Accordingly, we applied a recently developed redox 2D-DIGE methodology utilizing iodoacetylated ICy dyes [25] to assess UVB-induced changes in protein thiol reactivity. Briefly, UVB-irradiated (80 and 320 mJ/cm^2) or unirradiated cells were lysed in the presence of ICy5 in triplicate. Individual ICy5-labeled samples were then run on 2D gels against an equal load of ICy3-labeled standard pool comprising of an equal mixture of both sample types to aid in spot matching and to improve the accuracy of quantification (Fig. 6). The ICy5-labeled samples were subsequently labeled with lysine labeling Cy2 dye as an internal protein level control which was used to normalize the corresponding ICy5/ICy3 signals (Table 3). 1248 protein features were detected, of which 184 displayed statistically significant differences in labeling due to UVB irradiation. Notably, comparison of our saturated cysteine labeling strategy with that used for the minimal lysine labeling strategy in this study revealed increased protein precipitation at cysteine labeling 2D-DIGE above >70 kDa molecular weight range. This might be caused by the rise in the amount of ICy dye-modified cysteines in higher molecular weight proteins which leads to increased protein precipitation (data not shown). CCB post-staining and matching with fluorescence images allowed confident picking of 94 gel features and 37 of these were identified as unique gene products by MALDI-TOF peptide mass fingerprinting (Table 3). All of the identified proteins contain at least one cysteine, and since the ICy dyes target reduced cysteinyl thiols, these results suggest that UVB irradiation has altered the oxidative status of some of these thiol groups. These identified proteins were classified according to their subcellular locations and biological functions. 49% of the total proteins identified in CCD-966SK cells were cytosolic proteins. 16% of these identified proteins were membrane proteins and the other 16% were nucleus proteins. In addition, 11% of the identified proteins were located in mitochondria, 5% of identified proteins were secreted proteins and 3% of them were located in ER. Most of these identified proteins were involved in cytoskeleton (19%), metabolism (16%),

Table 2 – Representative list of proteins potentially contribute to protein folding, redox regulation, protein degradation, protein biosynthesis, cell migration, adhesion, nucleotide biosynthesis, growth regulation and calcium-dependent regulation in comparing CCD-966SK cells with/without UVB irradiation.

Functional class	Trend	Examples
Protein folding	↗	Peptidyl-prolyl cis-trans isomerase A; nucleophosmin; protein disulfide-isomerase
	↓	Heat shock protein beta-1/HSP-27
Redox regulation	↗	Peroxiredoxin-1; peroxiredoxin-4
Protein degradation	↓	E3 SUMO-protein ligase PIAS1
Protein biosynthesis	↓	40S ribosomal protein SA; heterogeneous nuclear ribonucleoproteins C1/C2
Cell migration	↑	Cofilin-1; fascin
Adhesion	↑	Otoancorin
Nucleotide biosynthesis	↑	Bifunctional purine biosynthesis protein PURH
Growth regulation	↑	Prohibitin
Calcium-dependent regulation	↑	Annexin A5; reticulocalbin-1
	↓	Annexin A2

signal transduction (13%), growth regulation (8%) and gene regulation (8%) (Fig. 7).

The UVB irradiation-induced alteration of thiol-reactivity was further validated by IP-WB. Prohibitin is one of the identified proteins with significant change in thiol reactivity under UVB irradiation. The thiol-reactivity of prohibitin was monitored by immunoprecipitation of ICy dye-labeled CCD-966SK cells irradiated with various doses of UVB and scanned the fluorescent images using an Ettan DIGE Imager. Subsequently, immunoblotting analysis was using the same primary antibody to measure the expression levels of prohibitin. The observed thiol reactivity of prohibitin was normalized with the expression level of the protein from immunoblotting to accurately measure the UVB-induced alteration in thiol reactivity (Fig. 8).

4. Discussion

Over the past few decades, the rapid progress of science and technology has resulted in a thinning of the ozone layer and an increase in solar UVB radiation reaching the earth. In humans, the skin is the first and only line of defense protecting the body from harmful UVB irradiation. Although the clinical symptoms of UVB damage (such as skin cancer) are well known, the molecular mechanisms causing this damage require further elucidation. Various approaches have been used to investigate the biological effects of UVB exposure on human skin, specifically on gene and protein expression levels [26–28]. The current study monitored UVB irradiation-induced alterations in the protein expression and thiol reactivity of skin fibroblasts, using lysine- and cysteine-labeling 2D-DIGE respectively. The protein expression profile identified 89 proteins that showed different expression levels in UVB-treated CCD-966SK cells compared with non-irradiated cells. Most of these proteins exhibited UVB dose-dependent protein expression changes between sham irradiation and UVB irradiations. However, almost a quarter of the identified proteins, such as peroxiredoxin-1, failed to display UVB dose-dependency for high dose UVB irradiation. This finding implied that high dose UVB might activate as-yet unknown mechanisms to protect skin cells from UVB-damage.

For changes in thiol reactivity, we identified 37 proteins showing redox-alterations of cysteine residues on specific proteins during UVB irradiation. This finding implied that UVB-induced oxidative stress disturbed the normal redox balance, and shifted CCD-966SK into a state in which the redox-modulation of specific proteins was systematically taking place. The ICy labeling results supported the hypothesis that UVB irradiation induces the formation of free thiols in certain proteins through disrupting disulphide bonds. In addition, UVB irradiation-induced reactive oxygen species (ROS) or protein-derived peroxides may directly oxidize thiol groups to form the sulfenic, sulfinic, or sulfonic acid forms of cysteine, which do not react with ICy dyes. These thiol modifications have been reported to perturb the normal functions of the proteins [29]. We thus suggest that UVB-induced regulation of protein expression combining redox-modification significantly influences cell physiology, and might contribute to the early progression of skin cancer formation.

The accumulation of damaged and misfolded proteins following toxic stimuli constitutes a major phenomenon in cells. Our results showed that many chaperone proteins and folding-related proteins were up-regulated under a medium dose of UVB exposure. These proteins included heat shock cognate 71 kDa protein, peptidyl-prolyl cis-trans isomerase A, nuclelophosmin, protein disulfide-isomerase, and calreticulin. Such proteins might be able to alleviate UVB-induced cell damage. The folding-related chaperone proteins were down-regulated under high doses of UVB irradiation. This finding might indicate that high-dose UVB irradiation caused direct damage to chaperone proteins, which then lost their ability to regenerate, or that the exposure may have induced caspase-3 protease-dependent cell apoptosis, which catalyzes the cleavage of many cellular proteins [30].

Nucleophosmin (NPM; also known as B23, NO38) is a nucleolar acidic chaperone protein that translocates to the cytoplasm during cellular stress. NPM is over-expressed in numerous cancers, such as gastric, colon, ovarian, and prostate carcinomas. Prior research has reported that UVC damages DNA, thereby increasing the activation of NPM promoters and stimulating NPM expression [31]. The activation of the Ras pathway after UV irradiation prolongs the half-life of c-Myc and enhances c-Myc activity, which allows the elevated c-Myc to bind to the promoter of NPM and up-regulates its transcript level [32,33]. In addition, NPM could interact with p53 and block p53 transcriptional activity, which would further inhibit cell apoptosis [34]. Furthermore, ARF is a tumor suppressor that inhibits the Mdm2-mediated p53 degradation. NPM targets ARF in nucleoli and prevents its binding to Mdm2. Released Mdm2 further ubiquitinates p53, which causes the rapid degradation of p53 and contributes to anti-apoptosis and tumor progression [35,36]. One study reported that NPM plays a role as an NF-κB co-activator and controls the cell cycle progression [37]. All these studies have suggested that

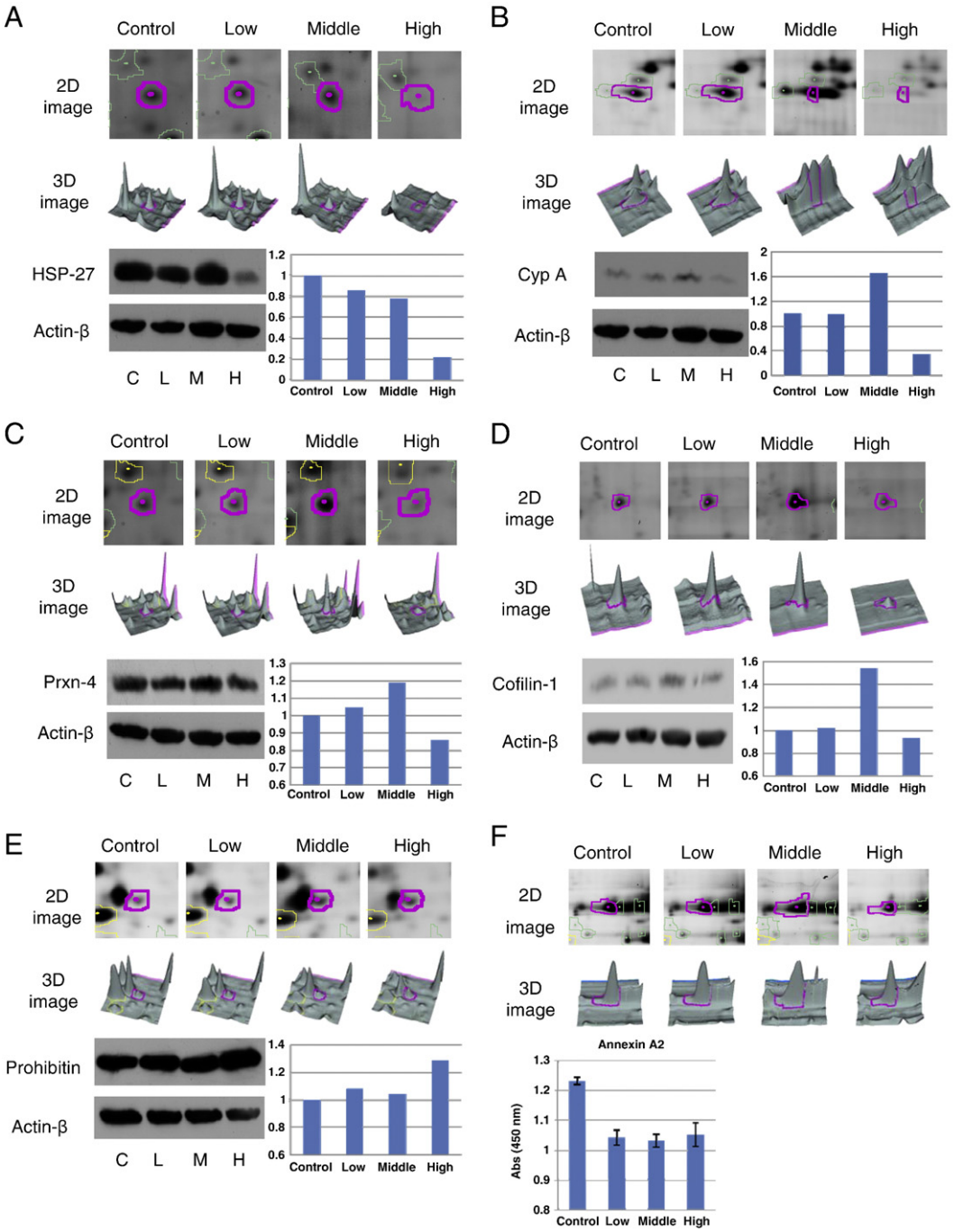

Fig. 4 – Representative immunoblotting and ELISA analyses for selected differentially expressed proteins identified by 2D-DIGE/MALDI-TOF MS for UVB-untreated or -irradiated CCD-966SK cells. The levels of identified proteins, (A) HSP-27, (B) cyclophilin A, (C) peroxiredoxin 4, (D) cofilin-1, (E) prohibitin in indicated doses of UVB-irradiated CCD-966SK cells versus untreated ones confirmed by immunoblot, densitometry results with normalized values using actin-β as loading controls, protein expression map and three-dimensional spot image. (F) 50 μg of UVB-irradiated CCD-966SK cells and untreated ones were coated onto each well of a 96-well plate for ELISA analysis with anti-annexin A2 antibody and absorbance was measured at 450 nm using a Stat Fax 2100 microtiter plate reader.

UVB induces NPM overexpression in CCD-966SK cells, which might contribute to skin cancer formation by stimulating anti-apoptosis and controlling the cell cycle (Fig. 9).

Heat shock proteins (HSPs) are molecular chaperones that accelerate cell recovery from harmful conditions, by reducing the concentrations of unfolded or denatured proteins [38]. The expression of HSP70 is induced by environmental and physiological stress, including UV irradiation and oxidative stress [39]. A recent study showed that HSP70 can inhibit the JNK/Bim signaling pathway and block the translocation of Bax to

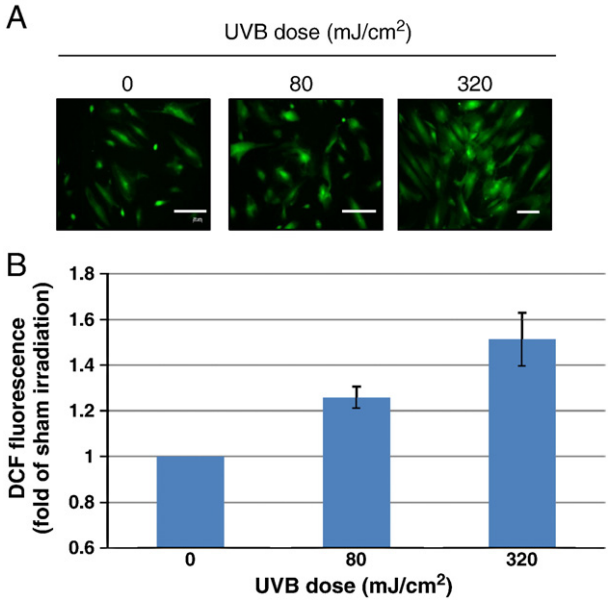

Fig. 5 – Effect of UVB on CCD-966SK ROS production. (A) DCFH-based intracellular ROS production assays were performed where 10,000 CCD-966SK cells were plated into 96-well plates in medium containing 10% FBS. After 24 h, the cells were irradiated with the indicated doses of UVB. Cells were then treated with 10 μM of DCFH-DA at 37 °C for 20 min and the fluorescence images was recorded at excitation and emission wavelengths of 485 nm and 530 nm, respectively. Each set of three fields was taken using the same exposure, and images are representative of three different fields. Scale bar=20 μm. (B) Microtiter plate-based DCFH analysis of intracellular ROS production assays were performed where MCF-7 cells were plated into 24-well plates. After 24 h, the cells were treated with the indicated dose of UVB. Cells were then treated with 10 μM of DCFH-DA at 37 °C for 20 min and the fluorescence was recorded at excitation and emission wavelengths of 485 nm and 530 nm, respectively.

mitochondria in UV-induced apoptosis. HSP70 also inhibits Bax activation by directly interacting with Bax, which prevents cytochrome c release from mitochondria and leads to anti-apoptosis in UV-irradiated cells [40]. Our data revealed that the over-expression of HSP70 in UVB-irradiated CCD-966SK cells played a role in promoting cell survival, and caused carcinogenesis by its anti-apoptotic function (Fig. 9).

Protein disulfide isomerase (PDI) is a ubiquitously expressed multifunctional protein that catalyzes the formation and rearrangement of disulfide bonds; it is involved in cell adhesion, gene regulation, cell–cell interaction, and actin filament polymerization [41]. UVB exposure induces the accumulation of unfolded or misfolded proteins in endoplasmic reticulum (ER), which causes ER stress and leads to mitochondrial cytochrome c release, leading to cell apoptosis [42,43]. Past studies have reported that PDI-knockdown or inhibition of PDI activity activates apoptotic signaling in cancer cells [44,45]. Thus PDI has been recognized as a protein that can protect cells from ER stress and stimulate cell survival. The results of the current study revealed increased levels of PDI in CCD-966SK cells after UVB irradiation, which might be an early event of skin cancer initiation. In addition, PDI participates in integrin-dependent cell adhesion and is highly expressed on migrating and invasive cancer cells [46]. Hence, the up-regulated PDI observed in our experiment might induce the formation of melanoma, which possesses the highly invasive ability of skin cancers (Fig. 9).

Endoplasmic reticulum plays a role in regulating intracellular calcium (Ca^{2+}) concentrations. ER stress might contribute to Ca^{2+} release from the ER and stimulate mitochondria disruption, which would influence cell apoptosis [47]. In the current study, this mechanism may explain why many calcium-dependent regulated proteins (including reticulocalbin-1, hippocalcin-like protein 1, and annexin A2 and A5) were identified with a distinct expression change in UVB-irradiated CCD-966SK cells compared to the non-irradiated cells (Fig. 9).

Cyclophilin A (Cyp A) was found to be up-regulated in our study. Cyp A displays peptidyl prolyl isomerase activity, which facilitates protein folding, assembly, and trafficking. It maintains the correct conformation of proteins and protects cells from the damage of environmental stress [48]. Numerous reports reveal that Cyp A is highly expressed in many cancers, and that Cyp A plays a role in blocking apoptosis, inducing proliferation, regulating metastasis, and controlling signaling pathways [49,50]. Jin et al. first demonstrated that Cyp A is a secreted mediator that responded to oxidative stress in cells [51]. Secreted Cyp A has been reported as a growth factor that can interact with the membrane receptor CD147 and stimulate phosphorylation of signaling molecules, including ERK, JNK, Akt, and IκB, thus leading to cell proliferation and migration [52]. In addition, Cyp A protects cells against oxidative stress-induced apoptosis [53]. The studies mentioned here indicated that UVB irradiation might contribute to tumor progression by up-regulating Cyp A, a hypothesis consistent with our own proteomic data (Fig. 9).

The redox-proteomic analysis of the current study found that proteins played a role in the redox-regulation of CCD-966SK cells. Specifically, identified redox-modulated proteins such as pyruvate kinase isozymes M1/M2 was up-regulated under medium doses of UVB irradiation but were down-regulated under high doses. These trends were identical to those of the earlier chaperone proteins. It might be that extreme UVB irradiation caused direct damage to these proteins, which thus lost their ability to regenerate. The redox-regulated proteins identified in the current study, including Prxn-1 and Prxn-4, are reportedly induced by oxidative stress. UVB irradiation causes the generation of ROS and results in oxidative stress in cells. Oxidative stress stimulates mitochondrial cytochrome c release and leads to apoptosis [54]. PRDXs are antioxidants with peroxidase activity that scavenge intracellular ROS and abolish ROS-induced apoptosis [55]. Thus, the over-expression of peroxiredoxins might contribute to UVB-induced skin cancers (Fig. 9).

Our findings also revealed that prohibitin (PHB) was up-regulated in CCD-966SK cells treated with high doses of UVB. PHB is a ubiquitously expressed protein that displays diverse functions at different locations. PHB is located in the inner membrane of mitochondria, and functions as a chaperone protein that maintains the morphology of mitochondria and

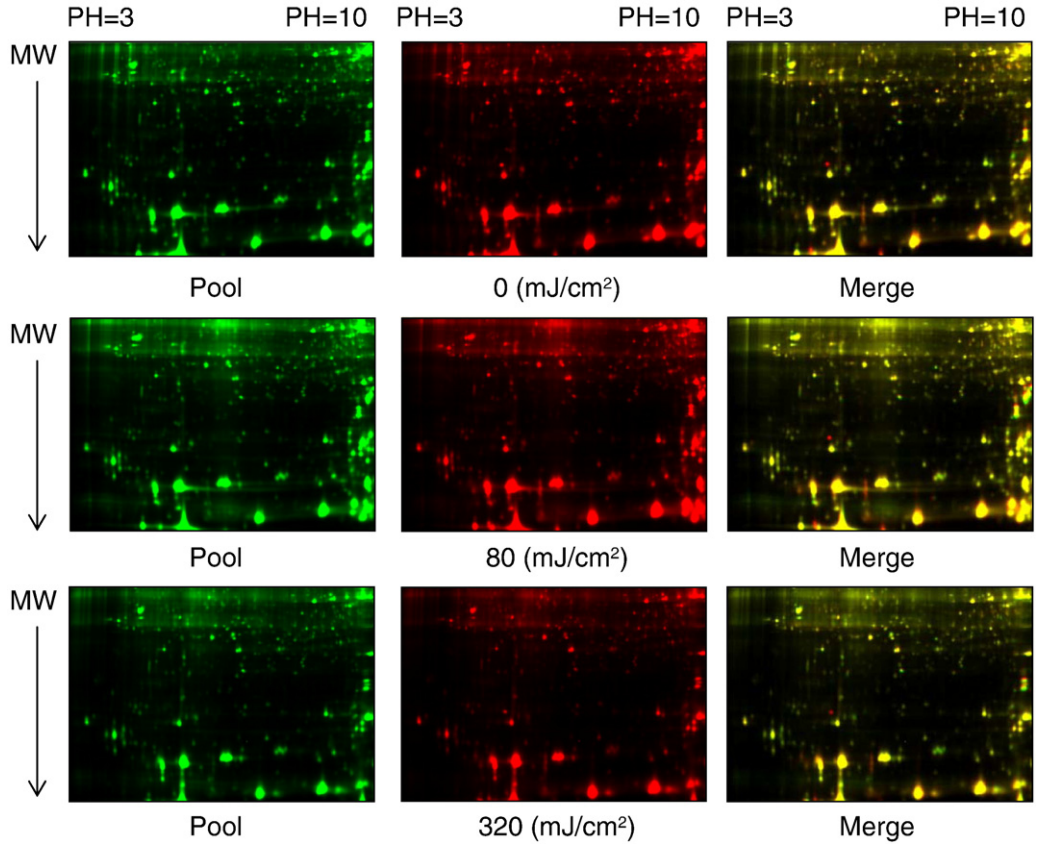

Fig. 6 – Redox 2D-DIGE analysis of UVB-induced differential cysteine-modification in CCD-966SK cells. Lysates from CCD-966SK cells irradiated with 80 mJ/cm^2 and 320 mJ/cm^2 of UVB or left untreated were subjected to redox 2D-DIGE analysis as described in Materials and methods. Images of protein samples from untreated and UVB-irradiated CCD-966SK are displayed.

stabilizes mitochondrial DNA [56]. Knock-down of PHB reduced the mitochondrial membrane potential and abolished complex I activity [57]. Recent research also suggests that the absence of PHB results in excessive ROS formation, which indicates that PHB might be important for the removal of ROS and inducing apoptosis [58]. PHB plays a role in transcriptional regulation, which is essential for cell proliferation and cell cycle regulation in the nucleus [59]. Additionally, PHB is highly expressed in many tumors. The expression of PHB is induced by c-Myc which might be stimulated by UVB-induced Ras activation. PHB directly interacts with Raf, which is essential for the membrane localization and phosphorylation of Raf. Then Ras activates the PHB–Raf complex to further activate the MEK–ERK cascades which modulate cell proliferation and migration [60]. Moreover, PI3K/AKT phosphorylates PHB on Thr258 and reduces Raf inhibition, thus promoting cell proliferation. The phosphorylation of PHB on Thr258 contributes to feedback that activates the PI3K/AKT pathway, leading to mitogenesis [61].

Interestingly, the residues of PHB are able to perform various types of post-translational modifications including phosphorylation, nitrosylation, cysteine oxidation, palmitoylation and transamidation, which are modulated with multiple cellular functions [62]. Our study indicated that the normalized free thiol level of PHB was increased in UVB-irradiated CCD-966SK cells, implying PHB has a reductive response on the cysteine residue during UVB irradiation. Importantly, PHB had only one cysteine residue at position 69, suggesting that Cys 69 was reduced under UVB irradiation. Previous research by Ande and Mishra demonstrated that cysteine palmitoylation at Cys 69 of PHB lead to its membrane translocation and interaction with Eps 15 homology domain protein 2, and affected cell signaling by facilitating tyrosine phosphorylation [63]. Although the detailed mechanism of Cys 69 requires further investigation, we propose that the post-translational modification of this cysteine residue might at least disturb the tyrosine phosphorylation signaling and membrane translocation ability of PHB (Fig. 9).

In this study, we also found that proteins possessing a nucleotide biosynthesis function showed a significant increase in UVB-irradiated CCD-966SK cells compared with control cells. These proteins contain bifunctional purine biosynthesis protein PURH, purine nucleoside phosphorylase, and UMP–CMP kinase. Elevated rates of nucleotide biosynthesis are crucial in cancer cells. The proliferation of cancer cells relies on the increase of nutrient uptake and the stimulation of signal transduction pathways to support nucleotide biosynthesis [64]. Accordingly, the up-regulation of nucleotide biosynthetic

Table 3 – Differential cysteine labeled proteins identified by ICy 2D-DIGE and MS. Proteins displaying UVB-induced differential labeling of cysteines and lysines using ICy dyes and NHS-Cy2 dyes, respectively, were identified by MALDI-TOF peptide mass mapping and MS/MS sequence analysis. Proteins displaying an average fold-difference of ≥1.3-fold where $p<0.05$ and spots matched in all images are shaded gray.

Accession no.	Protein name	MW	pI	No. matched peptides	Score	Cov. (%)	80 / ctrl[a]	320 / ctrl[a]	320 / 80[a]	Matched peptides	Subcellular location	Functional classification
P11021	78 kDa glucose-regulated protein	72,402	5.07	6/12	70	12%	1.41	1.07	–1.31	R.ITPSYVAFTPEGER.L, K.VTHAVVTVPAYFNDAQR.Q	ER	Protein folding
P24752	Acetyl-CoA acetyltransferase, mitochondrial	45,456	8.98	5/11	63	21%	1.35	1.18	–1.13	K.EAYMGNVLQGGEGQAPTR.Q, R.NEQDAYAINSYTR.S	Mitochondrion	Metabolism
P6070 9	Actin, cytoplasmic1	42,052	5.29	9/25	83	29%	1.26	1.92	1.53	K.AGFAGDDAPR.A, R.AVFPSIVGRPR.H	Cytoplasm	Cytoskeleton
P60709	Actin, cytoplasmic 1/ Actin, cytoplasmic 2	42,052	5.29	8/22	73	26%	1.29	1.62	1.25	R.AVFPSIVGRPR.H, K.IWHHTFYNELR.V	Cytoplasm	Cytoskeleton
P60709	Actin, cytoplasmic 1/ Actin, cytoplasmic 2	42,052	5.29	8/23	86	29%	–1.11	1.57	1.75	K.AGFAGDDAPR.A, R.AVFPSIVGRPR.H	Cytoplasm	Cytoskeleton
P60709	Actin, cytoplasmic 1/ Actin, cytoplasmic 2	42,052	5.29	7/27	77	23%	1.14	1.40	1.22	K.IWHHTFYNELR.V, R.VAPEEHPVLLTEAPLNPK.A	Cytoplasm	Cytoskeleton
Q9Y6K8	Adenylate kinase isoenzyme 5	22,358	5.38	4/11	58	29%	1.93	1.69	–1.14	K.YGFTHLSTGELLR.E, K.LIRDIMER.G	Cytoplasm	Signal transduction
P07355	Annexin A2	38,808	7.57	6/11	64	18%	–1.30	–1.20	1.09	K.AYTNFDAER.D, K.GVDEVTIVNILTNR.S	Plasma membrane	Signal transduction/Ca regulation
O00299	Chloride intracellular channel protein 1	27,248	5.09	5/11	70	19%	1.40	2.01	1.45	K.IGNCPFSQR.L, K.IEEFLEAVLCPPR.Y	Nucleus membrane	Redox regulation
P2352 8	Cofilin-1	18,719	8.22	4/8	56	26%	1.31	–1.10	–1.44	K.AVLFCLSEDKK.N, K.MLPDKDCR.Y	Cytoplasm	Cell migration
	Complement C1q tumor									R.QGHPGIPGNPGHNGLPGR.D,		

P0C862	necrosis factor-related protein 9	34,831	8.59	4/7	60	15%	1.47	−1.26	−1.86	R.GSPGKHGPK.G	Secreted	Signal transduction
P46527	Cyclin-dependent kinase inhibitor 1B	22,288	6.54	4/9	60	22%	−1.17	1.23	1.43	R.VSNGSPSLER.M, R.MDARQAEHPKPSACR.N	Nucleus and cytoplasm	Cell cycle regulation
Q8N4W6	DnaJ homolog subfamily C member 22	38,176	9.39	5/8	60	18%	−1.05	1.49	1.54	R.QSPRGVTPPLSPIR.F, R.QSPRGVTPPLSPIR.F	Membrane	Protein folding
Q15024	Exosome complex exonuclease RRP42	32,442	5.08	4/8	58	19%	1.02	1.50	1.48	K.VYIVHGVQEDLR.V, R.GGDDLGTEIANTLYRIFNNK.S	Nucleus	Gene regulation
P52907	F-actin-capping protein subunit alpha-1	33,073	5.45	5/9	78	27%	2.10	1.77	−1.18	K.FITHAPPGEFNEVFNDVR.L, R.LLLNNDNLLR.E	Cytoplasm	Cytoskeleton
Q9C0E4	Glutamate receptor-interacting protein 2	113,344	6.06	8/15	60	7%	1.40	1.50	1.08	R.QSIPEEFRGITVVELIK.K, R.IISKTVDVSLYK.E	Cytoplasm	Synaptic transmission
P51991	Heterogeneous nuclear ribonucleoprotein A3	39,799	9.1	5/15	62	15%	−1.16	−1.68	−1.46	M.EVKPPPGRPQPDSGR.R, K.YGKIETIEVMEDR.Q	Nucleus	Gene regulation
Q8WYA0	Intraflagellar transport protein 81 homolog/ Carnitine deficiency-associated protein	80,038	8.9	8/16	66	12%	2.36	1.63	−1.44	K.QYEELMEAFKTLHK.E, K.TLHKEYEQLK.I	Membrane	Cilium formation
P02545	expressed in ventricle 1 Lamin-A/ C	74,380	6.57	8/18	63	12%	2.36	1.63	−1.44	R.SLETENAGLR.L, K.NIYSEELR.E	Nucleus	Nuclear membrane
P24844	Myosin regulatory light polypeptide 9	19,871	4.8	4/8	57	18%	−1.13	−1.56	−1.40	K.EAFNMIDQNR.D, R.FTDEEVDEMYR.E	Cytoplasm	Cytoskeleton
P30041	Peroxiredoxin-6	25,133	6	5/14	64	21%	−2.08	1.16	2.44	R.DFTPVCTTELGR.A, R.AAKLAPEFAK.R	Cytoplasm	Redox regulation
P07737	Profilin-1	15,216	8.44	6/16	73	36%	2.56	1.82	−1.42	R.SSFYVNGLTLGGQK.C, R.DSLLQDGEFSMDLR.T	Cytoplasm	Cytoskeleton
P35232	Prohibitin	29,843	5.57	7/26	86	37%	1.47	1.48	1.01	K.FGLALAVAGGVVNSALYNVD AGHR.A, K.DLQNVNITLR.I	Mitochondrion	Growth regulation

(*continued on next page*)

Table 3 *(continued)*

Accession no.	Protein name	MW	pI	No. matched peptides	Score	Cov. (%)	80 / ctrl[a]	320 / ctrl[a]	320 / 80[a]	Matched peptides	Subcellular location	Functional classification
A2A3K4	Protein tyrosine phosphatase domain-containing protein 1	85,543	7.35	6/11	60	8%	1.11	–1.47	–1.63	K.YHIIDQFLSHGIK.T, R.MTADQAIIFVRAK.R	Cytoplasm	Signal transduction
P14618	Pyruvate kinase isozymes M1/M2	58,470	7.96	7/23	92	17%	1.87	2.22	1.20	R.LDIDSPPITAR.N, R.NTGIICTIGPASR.S	Cytoplasm	Metabolism
P14618	Pyruvate kinase isozymes M1/M2	58,470	7.96	7/23	69	17%	–1.05	1.30	1.36	R.LDIDSPPITAR.N, R.NTGIICTIGPASR.S	Cytoplasm	Metabolism
P14618	Pyruvate kinase isozymes M1/M2	58,470	7.96	6/20	88	13%	1.49	1.57	1.05	R.LDIDSPPITAR.N, R.NTGIICTIGPASR.S	Cytoplasm	Metabolism
Q8WUD1	Ras-related protein Rab-2B	24,427	7.68	4/9	58	25%	1.38	1.14	–1.21	MTYAYLFKYIIIGDTGVGK.S, R.SITRSYYR.G	Cell membran	Protein transport
Q9274 3	Serine protease HTRA1	52,167	8.09	5/13	56	11%	1.06	1.59	1.48	R.LHRPPVIVLQR.G, K.IAPAVVHIELFR.K	Secreted	Signal transduction
Q9986 5	Spindlin-2A	29,284	6.72	5/14	58	23%	–1.16	–1.68	–1.46	M.KTPNAQEAEGQQTR.A, R.AAAGRATGSANMTK.	Nucleus	Cell cycle regulation
Q1424 7	Src substrate cortactin	61,770	5.24	6/11	61	12%	–2.03	–2.26	–1.11	K.LSKHCSQVDSVR.G, K.SAVGFDYQGKTEK.H	Cytoplasm	Growth regulation
Q1424 7	Src substrate cortactin	61,770	5.24	7/14	70	14%	–1.74	–2.21	–1.27	K.LSKHCSQVDSVR.G, K.SAVGFDYQGKTEK.H	Cytoplasm	Growth regulation
Q9P2R7	Succinyl-CoA ligase [ADP-forming] subunit beta	50,627	7.05	5/9	59	9%	–1.41	1.40	1.98	M.AASMFYGRLVAVATLR.N, R.LVAVATLR.N	Mitochondrion	Metabolism
Q9BYC2	Succinyl-CoA:3-ketoacid-coenzyme A transferase 2 / OXCT2	56,731	6.73	6/13	60	13%	1.17	1.34	1.13	R.CFATSPRLR.A, R.AKFYADPVEMVK.D	Mitochondrion	Metabolism
P37802	Transgelin-2	22,548	8.41	5/7	65	20%	1.97	2.09	1.06	R.GPAYGLSR.E, MSSPSPGK.R,	Plasma	Protein binding
P62256	Ubiquitin-conjugating enzyme E2H	20,699	4.55	4/11	60	28%	1.66	–1.29	–2.12	K.LIESKHEVTILGGLNEFVVK.F	Cytoplasm	Protein ubiquitination
O43309	Zinc finger and SCAN domain-containing protein 12	71,888	6.28	5/8	59	10%	–5.07	–2.51	2.03	M.ASTWAIQAHMDQDEPLEVK.I , K.EGEPSMSLQSMKAQPK.Y	Nucleus	Gene regulation

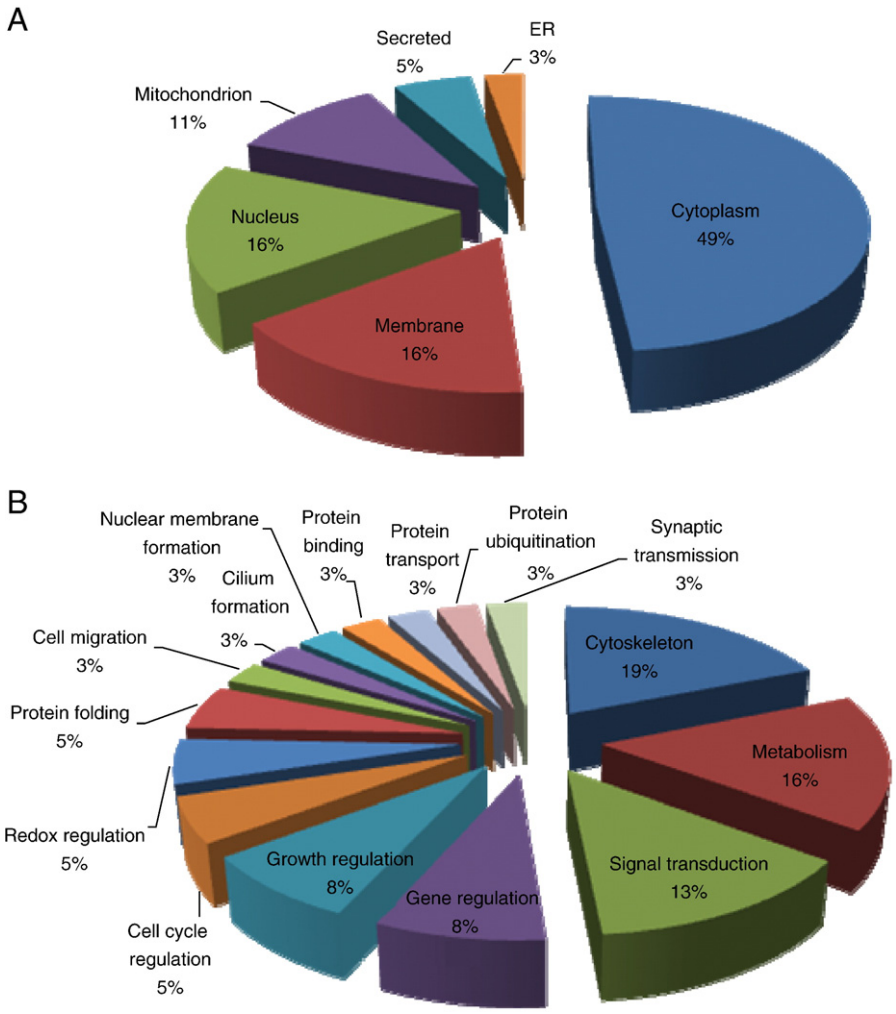

Fig. 7 – Distribution of differential ICy-labeled proteins from UVB-irradiated and untreated CCD-966SK cells according to (A) subcellular location and (B) biological function.

proteins might be an important molecular mechanism in the early stage of skin cancer formation (Fig. 9).

Metastasis is a major sign of malignancy and a driver of mortality in cancer patients. The process of metastasis, namely detachment from the primary tumor, intravasation, extravasation, and growth at another site, is controlled by the cytoskeleton [65,66]. Actin is one of the main cytoskeletal components that control cell motility and various cellular processes, such as endocytosis, cytokinesis, organelle transport, and cell signaling [67]. Actin-binding proteins (ABP) bind to actin and affect actin dynamics which regulate cytoskeletal organization and affect cell migration. Our study demonstrated that actin-binding proteins such as fascin and cofilin-1, and other cell migration-related proteins, were all over-expressed as a response to UVB irradiation.

Facin is an actin-binding protein that has been found in core actin bundles and localized to the leading edge of migratory cells. The over-expression of facin increases cell motility and correlates with several human cancers including breast, colon, ovary, and skin cancers [68]. In our proteomic study, facin was up-regulated under UVB-irradiation, revealing the early event of UVB-induced skin cancer formation (Fig. 9).

Cofilin-1 is an actin depolymerizing factor (ADF) that is responsible for the disassembly of actin filament. It controls actin filament dynamics and is essential for cell proliferation, migration, and cell cycle progression [69]. The deregulation of cofilin is associated with various tumors. Nowak et al. demonstrated that the expression level of cofilin distinctly increases in colon adenocarcinoma cells [70]. However, cofilin-1 activity is negatively regulated by phosphorylation. Previous research reported that UV induced the de-phosphorylation of cofilin-1 and activated the cofilin-1 function by altering kinase or phosphatase activity, which might be modulated by the UV-induced generation of ROS [71]. In addition, Klamt et al. found that oxidation of cofilin induced a loss of actin-binding ability and promoted cell apoptosis [72]. Our redox proteomic data indicated that cofilin-1 increased the labeling in normalized cysteine levels on UVB-irradiated CCD-966SK cells, implying that cofilin-1 was in a reductive state after UVB irradiation. This status might cause a rise in actin-

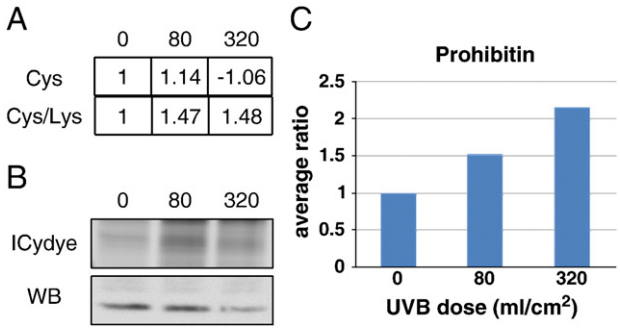

Fig. 8 – Validation of the thiol reactive protein, prohibitin, identified through redox-proteomic study in CCD-966SK cells after UVB irradiation by IP-WB. ICy dye-labeled protein samples from CCD-966SK cells were either untreated or treated with 80 and 320 mJ/cm^2 of UVB irradiation followed by immunoprecipitated with prohibitin antibody to confirm the alterations of thiol reactivity in prohibitin. The image was visualized by Ettan DIGE imager. Western blot against the corresponding antibody was performed to gain the protein level. (A) The relative ratio of cysteine level derived from DeCyder software and the cysteine level normalized with protein level of prohibitin are shown. (B) Prohibitin was validated by IP-WB. The ICy dye-labeled images were scanned by Ettan DIGE Imager (top panel). Protein level of prohibitin was obtained by Western blot analysis (bottom panel). (C) The relative ratio of cysteine level/protein level was calculated from ICy dye bands normalized with WB band intensities.

binding affinity and affect actin filament dynamics, inhibit cell apoptosis, and promote skin cancer formation (Fig. 9).

Profilin-1 and actin were up-regulated in the normalized cysteine level in our redox-proteomic data. Profilin-1 is an actin-binding protein contributing to actin filament assembly; it participates in morphogenesis, cytokinesis, embryonic development, and vesicle trafficking [73]. The binding affinity of profilin-1 is regulated by phosphorylation and oligomerization, but the function of reductive profilin is still unknown. Actin has been suggested as a redox-sensitive protein upon oxidative stress [74]. Dalle-Donne et al. showed that the oxidation of actin, such as S-glutathionylation, decreases the polymeric ability and reduces the elongation of actin filament [75]. Our data indicated that UVB-induced ROS caused the reduction of actin thiols in CCD-966SK cells, which might influence the interaction of actin with other factors and alter actin filament dynamics, inducing skin cancer formation (Fig. 9).

In our proteomic analysis, we observed that an adhesion-related protein, otoancorin, was up-regulated in CCD-966SK cells treated with UVB irradiation, and showed a UVB dose-dependent response. Otoancorin modulates the attachment of cellular gels and the apical surface of non-sensory cells in the inner ear [76]. Thus otoancorin might control actin filament dynamics and play a role in cell migration in UVB-irradiated CCD-966SK cells. Nevertheless, few prior reports have discussed the function of otoancorin, even its role in skin cancer progression.

The E3 SUMO-protein ligase PIAS1 belongs to the protein inhibitor of activated STATs (PIAS) family. We found that the expression of PIAS 1 was significantly decreased in CCD-966SK cells after UVB irradiation. PIAS 1 functions as a negative regulator of the JAK/STAT pathway in the nucleus, by negatively regulating methylation on STAT 1. PIAS 1 masks the DNA binding site and then blocks the cytokine-induced cellular response [77,78]. The JAK/STAT pathway is activated by the binding of cytokines to a specific receptor that constitutively connects with janus kinase (JNK). JNK is activated by dimerization and transphosphorylation. Activated JNK further phosphorylates the receptor, which recruits and phosphorylates signal transducers and activators of transcription 1 (STAT 1). Phosphorylated STAT 1 then dimerizes and translocates to the nucleus, leading to the binding of target genes which regulate cytokine-induced cellular responses including proliferation, differentiation, and survival [79,80] (Fig. 9). PIAS 1 also participates in DNA repair. Galanty et al. suggested that PIAS 1 accumulates at DNA double-strand break sites, which promotes the double-strand break signaling and induces the response of DNA repair [81]. In addition, Liu et al. reported that PIAS 1 directly interacts with NF-κB and inhibits cytokine-induced NF-κB activation [82]. In our study, PIAS 1 was down-regulated in CCD-966SK cells treated with UVB irradiation compared to the control cells. Down-regulated PIAS 1 might incur a suppressed inhibitive ability and induce the activation of the NF-κB and JAK/STAT pathways, prolonging skin cell growth and resulting in skin cancer formation (Fig. 9).

Skin aging is one of the most important features of solar radiation-induced damage, and is referred to as photoaging. Changes due to skin photoaging include wrinkling, elastosis, keratoses, pigmentation, and malignant skin tumors. The principle process of photoaging is the generation of ROS that cause an accumulation of damage. UVB-induced ROS activate transcription factors, such as activator protein-1 (AP-1), which increase the level of matrix metalloproteinase-1 (MMP-1), thereby stimulating collagen degradation and leading to skin photoaging [83] (Fig. 10). The expression of MMP-1 is also induced by the activation of cell surface receptor-induced signaling cascades such as the JAK/STAT and c-JNK pathways. This activation derives from the constitutive phosphorylation of EGFR by ROS-induced inhibition of protein tyrosine phosphatase (PTP) after UVB irradiation [84,85].

Skin pigmentation disorder is associated with a high risk of melanoma formation. This is due to the abnormal melanin produced by melanocytes [86]. Tanaka et al. reported that UV-induced NF-κB activation in skin fibroblasts triggers melanogenesis by the stimulation of COX-2 and endothelin expression. Activated NF-κB also induces the generation of basic fibroblast growth factor (bFGF), which is essential for the proliferation of melanocytes [87]. As a result, the proliferation of melanocytes increases the melanin formation and causes pigmentation which might lead to melanoma development (Fig. 10). According to our proteomic data, certain differentially expressed proteins contributed to cellular ROS level regulation, such as PRDXs and PHB, in UVB-irradiated CCD-966SK cells. These proteins might affect the cellular oxidative stress and participate in skin photoaging. We identified UVB-induced changes in the expression of proteins

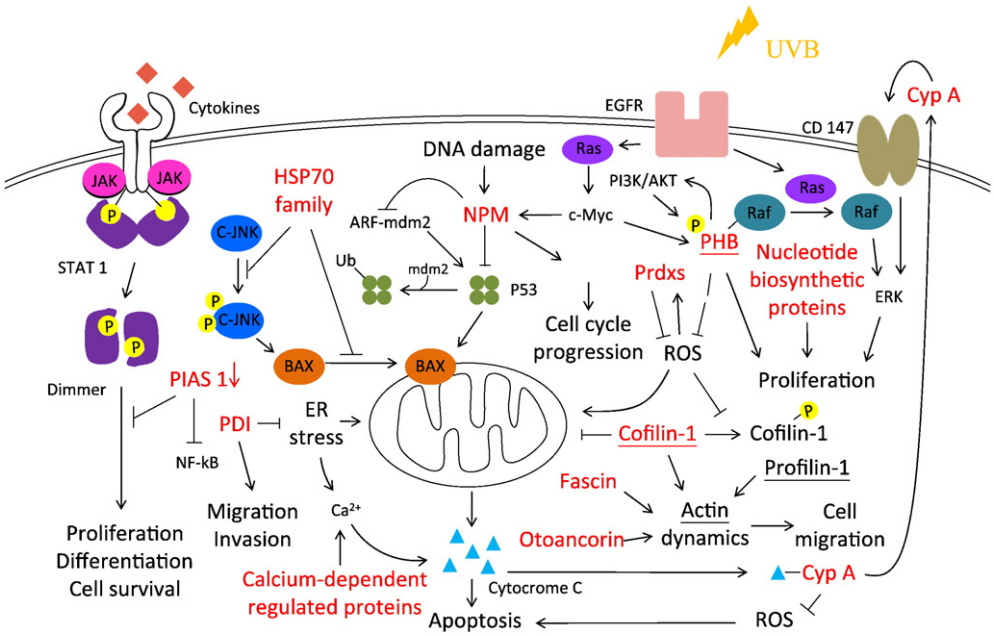

Fig. 9 – The hypothetical mechanisms of differentially expressed proteins derived from expression and redox proteomics in UVB-irradiated CCD-966SK cells. Results were compared with those of non-irradiated cells. Irradiation by UVB induced DNA damage, which promoted the activation of NPM promoter and stimulated NPM expression. NPM expression prolongs the half-life of c-Myc and enhances c-Myc activity. Elevated c-Myc binds to the promoter of NPM and up-regulates its transcript level. Thus, NPM could suppress the activation of p53 and further inhibit cell apoptosis. Moreover, NPM plays a role as NF-κB co-activator and controls the cell cycle progression. HSP70 may inhibit the JNK/Bim signaling pathway and block the translocation of Bax to mitochondria in UV-induced apoptosis. PDI has been identified as a protein that protects cells from ER stress and stimulates cell survival; it also participates in integrin-depended cell adhesion and is highly expressed on migrating and invasive cancer cells. UVB stress might contribute to Ca^{2+} release from ER and stimulate mitochondria disruption which participates in cell apoptosis. Cyp A inhibits the activation of cell apoptotic signaling by binding to released cytochrome c. Secreted Cyp A has been reported as a growth factor which interacts with membrane receptor CD147 and stimulates the phosphorylation of signaling molecules, including ERK, leading to cell proliferation and migration. PRDXs are antioxidants with peroxidase activity which scavenge intracellular reactive oxygen species. Prohibitin (PHB) is up-regulated under high doses of UVB, and plays a role in cell proliferation via activation of Ras-Raf-PI3K/Akt signaling. Proteins associated with nucleotide biosynthesis function showed a significant increase in nucleotide biosynthesis. Actin-binding proteins, such as fascin and cofilin-1, and other cell migration-related proteins were all over-expressed in response to UVB irradiation. Redox proteomic analysis showed that cofilin-1 was in a reductive state after UVB irradiation; this status might cause a rise in actin-binding affinity, affect the actin filament dynamics, and inhibit cell apoptosis. The UVB-induced ROS cause a reduction in actin and profiling-1 thiols, which might disturb the interaction of actin with other factors and alter actin filament dynamics. Otoancorin, an adhesion-related protein, was up-regulated under UVB irradiation and controlled the actin filament dynamics. The E3 SUMO-protein ligase PIAS1 was significantly down-regulated after UVB irradiation, leading to the activation of the JAK/STAT pathway in the nucleus via activation of STAT 1.UVB-irradiated proteins that displayed up-regulation in their expressed levels are shown in red in Fig. 9. Identified proteins with alterations in thiol reactivity are highlighted with baselines. Red arrows (↓) indicate the down-regulation of proteins.

including PISA 1, peroxiredoxins, PHB, NPM, HSP70, HSP27, and Cyp A. These proteins might play roles in skin photoaging by controlling the relative cellular signaling pathways. Interestingly, HSP27, one of chaperone proteins, was down-regulated in CCD-966SK cells treated with UVB irradiation compared to the non-irradiated cells. Similarly, Jonak et al. performed biopsies and found that the expression of HSP27 gradually decreased with age [88]. Our data revealed that HSP27 with low-expression levels might not only function as a chaperone protein but might also play an important role in photoaging in UVB-irradiated CCD-966SK cells (Fig. 10).

In summary, we performed comprehensive proteomic analysis after irradiating normal skin fibroblast cells with varying levels of UVB. We identified differentially expressed proteins, and attempted to develop a novel redox proteomic strategy to monitor the redox-modulated proteins in skin fibroblasts CCD-966SK after UVB exposure. These UVB-modulated proteins participate in many cellular responses including anti-apoptosis, tumorigenesis, cell migration,

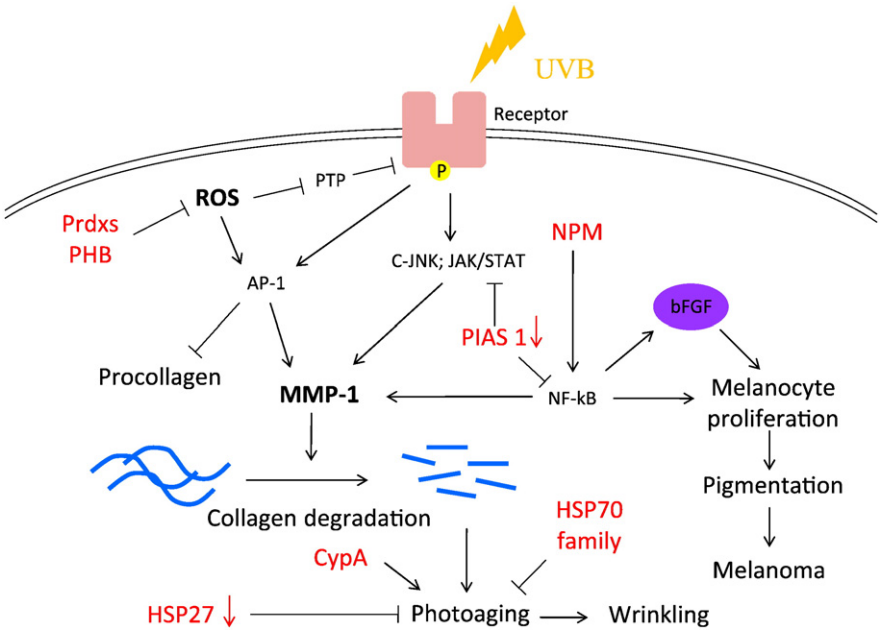

Fig. 10 – The hypothetical mechanisms of differentially expressed proteins involved in aging and melanogenesis in CCD-966SK cells irradiated with UVB. UVB-induced ROS activate transcription factors, such as activator protein-1 (AP-1), which increase the level of matrix metalloproteinase-1 (MMP-1) and thereby stimulate collagen degradation and lead to skin photoaging. In addition, AP-1 inhibits the expression of procollagen by sequestering proteins that are essential in procollagen formation. MMP-1 expression is also induced by the activation of cell surface receptor-induced signaling cascades, such as the JAK/STAT and c-JNK pathways. These cascades derive from the constitutive phosphorylation of EGFR by ROS-induced inhibition of PTP after UVB irradiation. The activated cell surface receptor, EGFR, sequentially activates AP-1, resulting in MMP-1 expression and causing photoaging. UV-induced NF-κB activation in skin fibroblasts triggers melanogenesis and induces the generation of basic fibroblast growth factor (bFGF), which is essential for the proliferation of melanocytes. The resulting proliferation of melanocytes increases melanin formation and causes pigmentation, which may lead to melanoma in skin cells. PRDXs and PHB might affect the cellular oxidative stress and participate in skin photoaging. PISA 1, NPM, HSP70, HSP27, and Cyp A might play roles in skin photoaging by controlling the relative cellular signaling pathways.UVB-irradiated proteins displaying up-regulation in their expressed levels are shown in red here. Red arrows (↓) indicate the down-regulation of proteins. Detailed functions of these proteins are mentioned in the discussion section of this paper.

photoaging, and melanogenesis. Our study indicated a whole network of identified proteins in UVB-irradiated skin cells, and deduced their roles in the early stage of skin cancer formation and photoaging. Our findings are pertinent to photoprotective cosmetics for repair of UVB-induced skin damage; in addition, the identified proteins might be potential targets for preventing UVB-induced tumorigenesis.

Declaration of competing interests

The authors confirm that there are no conflicts of interest.

Acknowledgments

This work was supported by NSC grant (100-2311-B-007-005) from National Science Council, Taiwan and Toward world-class university project from National Tsing Hua University, Taiwan.

REFERENCES

[1] Ibuki Y, Naitou H, Ohashi N, Goto R. Proteome analysis of UV-B-induced anti-apoptotic regulatory factors. Photochem Photobiol 2005;81:823–9.
[2] Lee E, Koo J, Berger T. UVB phototherapy and skin cancer risk: a review of the literature. Int J Dermatol 2005;44:355–60.
[3] de Gruijl FR. p53 mutations as a marker of skin cancer risk: comparison of UVA and UVB effects. Exp Dermatol 2002;11(Suppl. 1):37–9.
[4] Heck DE, Gerecke DR, Vetrano AM, Laskin JD. Solar ultraviolet radiation as a trigger of cell signal transduction. Toxicol Appl Pharmacol 2004;195:288–97.
[5] Ashida M, Bito T, Budiyanto A, Ichihashi M, Ueda M. Involvement of EGF receptor activation in the induction of cyclooxygenase-2 in HaCaT keratinocytes after UVB. Exp Dermatol 2003;12:445–52.
[6] Madson JG, Lynch DT, Tinkum KL, Putta SK, Hansen LA. Erbb2 regulates inflammation and proliferation in the skin after ultraviolet irradiation. Am J Pathol 2006;169:1402–14.
[7] Halliwell B. Oxidative stress and cancer: have we moved forward? Biochem J 2007;401:1–11.

[8] Valko M, Rhodes CJ, Moncol J, Izakovic M, Mazur M. Free radicals, metals and antioxidants in oxidative stress-induced cancer. Chem Biol Interact 2006;160:1–40.
[9] D'Autreaux B, Toledano MB. ROS as signalling molecules: mechanisms that generate specificity in ROS homeostasis. Nat Rev Mol Cell Biol 2007;8:813–24.
[10] Toyokuni S, Okamoto K, Yodoi J, Hiai H. Persistent oxidative stress in cancer. FEBS Lett 1995;358:1–3.
[11] Schafer FQ, Buettner GR. Redox environment of the cell as viewed through the redox state of the glutathione disulfide/glutathione couple. Free Radic Biol Med 2001;30: 1191–212.
[12] Lim JC, Choi HI, Park YS, Nam HW, Woo HA, Kwon KS, et al. Irreversible oxidation of the active-site cysteine of peroxiredoxin to cysteine sulfonic acid for enhanced molecular chaperone activity. J Biol Chem 2008;283:28873–80.
[13] Jacob C, Holme AL, Fry FH. The sulfinic acid switch in proteins. Org Biomol Chem 2004;2:1953–6.
[14] Herbert BR, Harry JL, Packer NH, Gooley AA, Pedersen SK, Williams KL. What place for polyacrylamide in proteomics? Trends Biotechnol 2001;19:3–9.
[15] Rabilloud T. Two-dimensional electrophoresis of basic proteins with equilibrium isoelectric focusing in carrier ampholyte-pH gradients. Electrophoresis 1994;15:278–82.
[16] Hung PH, Chen YW, Cheng KC, Chou HC, Lyu PC, Lu YC, et al. Plasma proteomic analysis of the critical limb ischemia markers in diabetic patients with hemodialysis. Mol Biosyst 2011;7:1990–8.
[17] Huang HL, Hsing HW, Lai TC, Chen YW, Lee TR, Chan HT, et al. Trypsin-induced proteome alteration during cell subculture in mammalian cells. J Biomed Sci 2010;17:36.
[18] Lai TC, Chou HC, Chen YW, Lee TR, Chan HT, Shen HH, et al. Secretomic and proteomic analysis of potential breast cancer markers by two-dimensional differential gel electrophoresis. J Proteome Res 2010;9:1302–22.
[19] Chen YW, Chou HC, Lyu PC, Yin HS, Huang FL, Chang WS, et al. Mitochondrial proteomics analysis of tumorigenic and metastatic breast cancer markers. Funct Integr Genomics 2011;11:225–39.
[20] Chou HC, Chen YW, Lee TR, Wu FS, Chan HT, Lyu PC, et al. Proteomics study of oxidative stress and Src kinase inhibition in H9C2 cardiomyocytes: a cell model of heart ischemia reperfusion injury and treatment. Free Radic Biol Med 2010;49:96–108.
[21] Perluigi M, Giorgi A, Blarzino C, De Marco F, Foppoli C, Di Domenico F, et al. Proteomics analysis of protein expression and specific protein oxidation in human papillomavirus transformed keratinocytes upon UVB irradiation. J Cell Mol Med 2009;13:1809–22.
[22] Chen YW, Liu JY, Lin ST, Li JM, Huang SH, Chen JY, et al. Proteomic analysis of gemcitabine-induced drug resistance in pancreatic cancer cells. Mol Biosyst 2011;7: 3065–74.
[23] Chan HL, Gaffney PR, Waterfield MD, Anderle H, Peter MH, Schwarz HP, et al. Proteomic analysis of UVC irradiation-induced damage of plasma proteins: serum amyloid P component as a major target of photolysis. FEBS Lett 2006;580:3229–36.
[24] Chan HL, Gharbi S, Gaffney PR, Cramer R, Waterfield MD, Timms JF. Proteomic analysis of redox- and ErbB2-dependent changes in mammary luminal epithelial cells using cysteine- and lysine-labelling two-dimensional difference gel electrophoresis. Proteomics 2005;5:2908–26.
[25] Timms JF, Cramer R. Difference gel electrophoresis. Proteomics 2008;8:4886–97.
[26] Enk CD, Shahar I, Amariglio N, Rechavi G, Kaminski N, Hochberg M. Gene expression profiling of in vivo UVB-irradiated human epidermis. Photodermatol Photoimmunol Photomed 2004;20:129–37.
[27] Howell BG, Wang B, Freed I, Mamelak AJ, Watanabe H, Sauder DN. Microarray analysis of UVB-regulated genes in keratinocytes: downregulation of angiogenesis inhibitor thrombospondin-1. J Dermatol Sci 2004;34:185–94.
[28] Bertrand-Vallery V, Belot N, Dieu M, Delaive E, Ninane N, Demazy C, et al. Proteomic profiling of human keratinocytes undergoing UVB-induced alternative differentiation reveals TRIpartite Motif Protein 29 as a survival factor. PLoS One 2010;5:e10462.
[29] Ghezzi P, Bonetto V, Fratelli M. Thiol-disulfide balance: from the concept of oxidative stress to that of redox regulation. Antioxid Redox Signal 2005;7:964–72.
[30] Porter AG, Janicke RU. Emerging roles of caspase-3 in apoptosis. Cell Death Differ 1999;6:99–104.
[31] Wu MH, Yung BY. UV stimulation of nucleophosmin/B23 expression is an immediate-early gene response induced by damaged DNA. J Biol Chem 2002;277:48234–40.
[32] Sears R, Leone G, DeGregori J, Nevins JR. Ras enhances Myc protein stability. Mol Cell 1999;3:169–79.
[33] Yung BY. Oncogenic role of nucleophosmin/B23. Chang Gung Med J 2007;30:285–93.
[34] Maiguel DA, Jones L, Chakravarty D, Yang C, Carrier F. Nucleophosmin sets a threshold for p53 response to UV radiation. Mol Cell Biol 2004;24:3703–11.
[35] Colombo E, Alcalay M, Pelicci PG. Nucleophosmin and its complex network: a possible therapeutic target in hematological diseases. Oncogene 2011;30:2595–609.
[36] Korgaonkar C, Hagen J, Tompkins V, Frazier AA, Allamargot C, Quelle FW, et al. Nucleophosmin (B23) targets ARF to nucleoli and inhibits its function. Mol Cell Biol 2005;25: 1258–71.
[37] Lin CY, Liang YC, Yung BY. Nucleophosmin/B23 regulates transcriptional activation of E2F1 via modulating the promoter binding of NF-kappaB, E2F1 and pRB. Cell Signal 2006;18:2041–8.
[38] Rohde M, Daugaard M, Jensen MH, Helin K, Nylandsted J, Jaattela M. Members of the heat-shock protein 70 family promote cancer cell growth by distinct mechanisms. Genes Dev 2005;19:570–82.
[39] Morimoto RI, Sarge KD, Abravaya K. Transcriptional regulation of heat shock genes. A paradigm for inducible genomic responses. J Biol Chem 1992;267:21987–90.
[40] Li H, Liu L, Xing D, Chen WR. Inhibition of the JNK/Bim pathway by Hsp70 prevents Bax activation in UV-induced apoptosis. FEBS Lett 2010;584:4672–8.
[41] Perluigi M, Di Domenico F, Blarzino C, Foppoli C, Cini C, Giorgi A, et al. Effects of UVB-induced oxidative stress on protein expression and specific protein oxidation in normal human epithelial keratinocytes: a proteomic approach. Proteome Sci 2010;8:13.
[42] Hacki J, Egger L, Monney L, Conus S, Rosse T, Fellay I, et al. Apoptotic crosstalk between the endoplasmic reticulum and mitochondria controlled by Bcl-2. Oncogene 2000;19:2286–95.
[43] Mera K, Kawahara K, Tada K, Kawai K, Hashiguchi T, Maruyama I, et al. ER signaling is activated to protect human HaCaT keratinocytes from ER stress induced by environmental doses of UVB. Biochem Biophys Res Commun 2010;397:350–4.
[44] Hashida T, Kotake Y, Ohta S. Protein disulfide isomerase knockdown-induced cell death is cell-line-dependent and involves apoptosis in MCF-7 cells. J Toxicol Sci 2011;36:1–7.
[45] Lovat PE, Corazzari M, Armstrong JL, Martin S, Pagliarini V, Hill D, et al. Increasing melanoma cell death using inhibitors of protein disulfide isomerases to abrogate survival responses to endoplasmic reticulum stress. Cancer Res 2008;68:5363–9.
[46] Goplen D, Wang J, Enger PO, Tysnes BB, Terzis AJ, Laerum OD, et al. Protein disulfide isomerase expression is related to the invasive properties of malignant glioma. Cancer Res 2006;66: 9895–902.

[47] Nakamura K, Bossy-Wetzel E, Burns K, Fadel MP, Lozyk M, Goping IS, et al. Changes in endoplasmic reticulum luminal environment affect cell sensitivity to apoptosis. J Cell Biol 2000;150:731–40.
[48] Kim IS, Kim HY, Shin SY, Kim YS, Lee DH, Park KM, et al. A cyclophilin A CPR1 overexpression enhances stress acquisition in Saccharomyces cerevisiae. Mol Cells 2010;29: 567–74.
[49] Lee J. Role of cyclophilin a during oncogenesis. Arch Pharm Res 2010;33:181–7.
[50] Choi KJ, Piao YJ, Lim MJ, Kim JH, Ha J, Choe W, et al. Overexpressed cyclophilin A in cancer cells renders resistance to hypoxia- and cisplatin-induced cell death. Cancer Res 2007;67:3654–62.
[51] Jin ZG, Melaragno MG, Liao DF, Yan C, Haendeler J, Suh YA, et al. Cyclophilin A is a secreted growth factor induced by oxidative stress. Circ Res 2000;87:789–96.
[52] Obchoei S, Wongkhan S, Wongkham C, Li M, Yao Q, Chen C. Cyclophilin A: potential functions and therapeutic target for human cancer. Med Sci Monit 2009;15:RA221–32.
[53] Doyle V, Virji S, Crompton M. Evidence that cyclophilin-A protects cells against oxidative stress. Biochem J 1999;341(Pt 1):127–32.
[54] Ueda S, Masutani H, Nakamura H, Tanaka T, Ueno M, Yodoi J. Redox control of cell death. Antioxid Redox Signal 2002;4: 405–14.
[55] Zhang B, Wang Y, Su Y. Peroxiredoxins, a novel target in cancer radiotherapy. Cancer Lett 2009;286:154–60.
[56] Osman C, Merkwirth C, Langer T. Prohibitins and the functional compartmentalization of mitochondrial membranes. J Cell Sci 2009;122:3823–30.
[57] Merkwirth C, Langer T. Prohibitin function within mitochondria: essential roles for cell proliferation and cristae morphogenesis. Biochim Biophys Acta 2009;1793:27–32.
[58] Schleicher M, Shepherd BR, Suarez Y, Fernandez-Hernando C, Yu J, Pan Y, et al. Prohibitin-1 maintains the angiogenic capacity of endothelial cells by regulating mitochondrial function and senescence. J Cell Biol 2008;180:101–12.
[59] Czarnecka AM, Campanella C, Zummo G, Cappello F. Mitochondrial chaperones in cancer: from molecular biology to clinical diagnostics. Cancer Biol Ther 2006;5:714–20.
[60] Rajalingam K, Wunder C, Brinkmann V, Churin Y, Hekman M, Sievers C, et al. Prohibitin is required for Ras-induced Raf-MEK-ERK activation and epithelial cell migration. Nat Cell Biol 2005;7:837–43.
[61] Han EK, Mcgonigal T, Butler C, Giranda VL, Luo Y. Characterization of Akt overexpression in MiaPaCa-2 cells: prohibitin is an Akt substrate both in vitro and in cells. Anticancer Res 2008;28:957–63.
[62] Mishra S, Ande SR, Nyomba BL. The role of prohibitin in cell signaling. FEBS J 2010;277:3937–46.
[63] Ande SR, Mishra S. Palmitoylation of prohibitin at cysteine 69 facilitates its membrane translocation and interaction with Eps 15 homology domain protein 2 (EHD2). Biochem Cell Biol 2010;88:553–8.
[64] Tong X, Zhao F, Thompson CB. The molecular determinants of de novo nucleotide biosynthesis in cancer cells. Curr Opin Genet Dev 2009;19:32–7.
[65] Xing P, Li JG, Jin F, Zhao TT, Liu Q, Dong HT, et al. Fascin, an actin-bundling protein, promotes breast cancer progression in vitro. Cell Biochem Funct 2011;29:303–10.
[66] Steeg PS, Theodorescu D. Metastasis: a therapeutic target for cancer. Nat Clin Pract Oncol 2008;5:206–19.
[67] Pollard TD, Cooper JA. Actin, a central player in cell shape and movement. Science 2009;326:1208–12.
[68] Qualtrough D, Singh K, Banu N, Paraskeva C, Pignatelli M. The actin-bundling protein fascin is overexpressed in colorectal adenomas and promotes motility in adenoma cells in vitro. Br J Cancer 2009;101:1124–9.
[69] Tsai CH, Chiu SJ, Liu CC, Sheu TJ, Hsieh CH, Keng PC, et al. Regulated expression of cofilin and the consequent regulation of p27(kip1) are essential for G(1) phase progression. Cell Cycle 2009;8:2365–74.
[70] Nowak D, Mazur AJ, Popow-Wozniak A, Radwanska A, Mannherz HG, Malicka-Blaszkiewicz M. Subcellular distribution and expression of cofilin and ezrin in human colon adenocarcinoma cell lines with different metastatic potential. Eur J Histochem 2010;54:e14.
[71] Hensbergen P, Alewijnse A, Kempenaar J, van der Schors RC, Balog CA, Deelder A, et al. Proteomic profiling identifies an UV-induced activation of cofilin-1 and destrin in human epidermis. J Invest Dermatol 2005;124:818–24.
[72] Klamt F, Zdanov S, Levine RL, Pariser A, Zhang Y, Zhang B, et al. Oxidant-induced apoptosis is mediated by oxidation of the actin-regulatory protein cofilin. Nat Cell Biol 2009;11:1241–6.
[73] Jockusch BM, Murk K, Rothkegel M. The profile of profilins. Rev Physiol Biochem Pharmacol 2007;159:131–49.
[74] DalleDonne I, Milzani A, Colombo R. H_2O_2-treated actin: assembly and polymer interactions with cross-linking proteins. Biophys J 1995;69:2710–9.
[75] Dalle-Donne I, Giustarini D, Rossi R, Colombo R, Milzani A. Reversible S-glutathionylation of Cys 374 regulates actin filament formation by inducing structural changes in the actin molecule. Free Radic Biol Med 2003;34:23–32.
[76] Zwaenepoel I, Mustapha M, Leibovici M, Verpy E, Goodyear R, Liu XZ, et al. Otoancorin, an inner ear protein restricted to the interface between the apical surface of sensory epithelia and their overlying acellular gels, is defective in autosomal recessive deafness DFNB22. Proc Natl Acad Sci U S A 2002;99: 6240–5.
[77] Schmidt D, Muller S. PIAS/SUMO: new partners in transcriptional regulation. Cell Mol Life Sci 2003;60:2561–74.
[78] Coccia EM, Stellacci E, Orsatti R, Benedetti E, Giacomini E, Marziali G, et al. Protein inhibitor of activated signal transducer and activator of transcription (STAT)-1 (PIAS-1) regulates the IFN-gamma response in macrophage cell lines. Cell Signal 2002;14:537–45.
[79] Starr R, Hilton DJ. Negative regulation of the JAK/STAT pathway. Bioessays 1999;21:47–52.
[80] Carbia-Nagashima A, Arzt E. Intracellular proteins and mechanisms involved in the control of gp130/JAK/STAT cytokine signaling. IUBMB Life 2004;56:83–8.
[81] Galanty Y, Belotserkovskaya R, Coates J, Polo S, Miller KM, Jackson SP. Mammalian SUMO E3-ligases PIAS1 and PIAS4 promote responses to DNA double-strand breaks. Nature 2009;462:935–9.
[82] Liu B, Yang R, Wong KA, Getman C, Stein N, Teitell MA, et al. Negative regulation of NF-kappaB signaling by PIAS1. Mol Cell Biol 2005;25:1113–23.
[83] Chen CL, Liou SF, Chen SJ, Shih MF. Protective effects of *Chlorella*-derived peptide on UVB-induced production of MMP-1 and degradation of procollagen genes in human skin fibroblasts. Regul Toxicol Pharmacol 2011;60:112–9.
[84] Masaki H. Role of antioxidants in the skin: anti-aging effects. J Dermatol Sci 2010;58:85–90.
[85] Kim S, Kim Y, Lee Y, Chung JH. Ceramide accelerates ultraviolet-induced MMP-1 expression through JAK1/STAT-1 pathway in cultured human dermal fibroblasts. J Lipid Res 2008;49:2571–81.
[86] Yamashita Y, Hoshino T, Matsuda M, Kobayashi C, Tominaga A, Nakamura Y, et al. HSP70 inducers from Chinese herbs and their effect on melanin production. Exp Dermatol 2010;19: e340–2.
[87] Tanaka K, Asamitsu K, Uranishi H, Iddamalgoda A, Ito K, Kojima H, et al. Protecting skin photoaging by NF-kappaB inhibitor. Curr Drug Metab 2010;11:431–5.
[88] Jonak C, Klosner G, Trautinger F. Heat shock proteins in the skin. Int J Cosmet Sci 2006;28:233–41.